POSSIBLE GRAVITATIONAL ANOMALIES IN QUANTUM MATERIALS
Phase I: Experiment Definition and Design

M. Tajmar and K. Hense

Austrian Research Centers Seibersdorf Research GmbH
A-2444 Seibersdorf, Austria

Award No. FA8655-03-1-3075

February 2007

FINAL REPORT FOR PERIOD August 2003 – February 2004

AIR FORCE RESEARCH LABORATORY, MUNITIONS DIRECTORATE
Air Force Materiel Command ■ United States Air Force ■ Eglin Air Force Base

NOTICE AND SIGNATURE PAGE

Using Government drawings, specifications, or other data included in this document for any purpose other than Government procurement does not in any way obligate the U.S. Government. The fact that the Government formulated or supplied the drawings, specifications, or other data does not license the holder or any other person or corporation; or convey any rights or permission to manufacture, use, or sell any patented invention that may relate to them.

This report was cleared for public release by the Air Armament Center Public Affairs Office and is available to the general public, including foreign nationals. Copies may be obtained from the Defense Technical Information Center (DTIC) (http://www.dtic.mil).

AFRL-MN-EG-TR-2007-7012 HAS BEEN REVIEWED AND IS APPROVED FOR PUBLICATION IN ACCORDANCE WITH ASSIGNED DISTRIBUTION STATEMENT.

FOR THE DIRECTOR:

// original signed //   *// original signed //*   *// original signed //*

DANNY R. HAYLES   KIRK E. HERZOG   DONALD M. LITTRELL
Technical Director   Technical Advisor   Program Manager
Ordnance Division   Damage Mechanisms Branch   Damage Mechanisms Branch

This report is published in the interest of scientific and technical information exchange, and its publication does not constitute the Government's approval or disapproval of its ideas or findings.

REPORT DOCUMENTATION PAGE

Form Approved
OMB No. 0704-0188

1. REPORT DATE *(DD-MM-YYYY)* February 2007	2. REPORT TYPE Final	3. DATES COVERED *(From - To)* August 2003 – February 2004

4. TITLE AND SUBTITLE POSSIBLE GRAVITATIONAL ANOMALIES IN QUANTUM MATERIALS Phase I: Experiment Definition and Design	5a. CONTRACT NUMBER
	5b. GRANT NUMBER FA8655-03-1-3075
	5c. PROGRAM ELEMENT NUMBER 62602F
6. AUTHOR(S) M. Tajmar and K. Hense Austrian Research Centers Seibersdorf Research GmbH A-2444 Seibersdorf, Austria	5d. PROJECT NUMBER 2502
	5e. TASK NUMBER 99
	5f. WORK UNIT NUMBER 14

7. PERFORMING ORGANIZATION NAME(S) AND ADDRESS(ES) Austrian Research Centers Seibersdorf Research GmbH A-2444 Seibersdorf, Austria	8. PERFORMING ORGANIZATION REPORT NUMBER

9. SPONSORING / MONITORING AGENCY NAME(S) AND ADDRESS(ES) Air Force Research Laboratory Munitions Directorate, AFRL/MNMW 101 W. Eglin Blvd., Ste. 135 Eglin AFB FL 32542-6810	10. SPONSOR/MONITOR'S ACRONYM(S) AFRL-MN-EG
	11. SPONSOR/MONITOR'S REPORT NUMBER(S) AFRL-MN-EG-TR-2007-7012

12. DISTRIBUTION / AVAILABILITY STATEMENT
DISTRIBUTION A: Approved for public release; distribution unlimited. AAC/PA Approval and Clearance # 01-12-07-015, dated 12 January 2007.

13. SUPPLEMENTARY NOTES

14. ABSTRACT: One of the authors (MT) recently published a paper, suggesting for the first time that a reported disagreement between experimental measurements and theoretical predictions for the magnetic field in rotating superconductors might arise from an anomalous high-order gravitomagnetic contribution (also known as frame dragging or Lense-Thirring effect). In normal matter, the ratio between electromagnetic and gravitational fields is given by the difference in the respective permeabilities. However, magnetic fields generated as a consequence of the quantization of the canonical momentum in a superconductor do not depend on the permeability. Hence, there is the possibility that the ratio between those two fields might be different in a quantum material.

This report summarizes the work carried out in Phase I – the experiment definition, detailed analysis and design. According to the performed analysis, the experimental apparatus described in this report is be able to resolve the gravitational anomaly having an ultimate resolution of 0.3 µg and exceeding the required rotational speeds and angular accelerations.

15. SUBJECT TERMS
gravitational anomaly, superconductor, frame dragging, Lense-Thirring effect, quantum material, magnetic field, gravity

16. SECURITY CLASSIFICATION OF:			17. LIMITATION OF ABSTRACT	18. NUMBER OF PAGES	19a. NAME OF RESPONSIBLE PERSON Donald M. Littrell
a. REPORT UNCLASSIFIED	b. ABSTRACT UNCLASSIFIED	c. THIS PAGE UNCLASSIFIED	SAR	57	19b. TELEPHONE NUMBER *(include area code)*

Standard Form 298 (Rev. 8-98)
Prescribed by ANSI Std. Z39.18

PREFACE

Dr. Martin Tajmar of the Austrian Research Centers (ARC) Seibersdorf presented a briefing on this subject at the Air Force Research Laboratory, Munitions Directorate (AFRL/MN), Eglin Air Force Base, Florida in the Fall of 2002 under the Window on Science (WOS) program managed by the European Office of Aerospace Research and Development (EOARD, Det. 1, AFOSR). ARC Seibersdorf submitted a formal proposal through AFOSR Broad Agency Announcement (BAA) 2003-1, and AFRL/MN sent a Military Departmental Purchase Request (MIPR) to EOARD on 1 August 2003 to fund the project. EOARD performed the contracting functions and AFRL/MN performed the programmatic and technical management functions.

This report documents the first phase of this project. The second phase is documented in AFRL/MN technical report AFRL-MN-EG-TR-2007-7013, "Possible Gravitational Anomalies in Quantum Materials, Phase II: Experiment Assembly, Qualification and Test Results," by M. Tajmar, February 2007.

Possible Gravitational Anomalies in Quantum Materials

Phase I: Experiment Definition and Design

Prepared by: M. Tajmar and K. Hense, ARC Seibersdorf research

ABSTRACT

One of the authors (MT) recently published a paper, suggesting for the first time that a reported disagreement between experimental measurements and theoretical predictions for the magnetic field in rotating superconductors might arise from an anomalous high-order gravitomagnetic contribution (also known as frame dragging or Lense-Thirring effect). In normal matter, the ratio between electromagnetic and gravitational fields is given by the difference in the respective permeabilities. However, magnetic fields generated as a consequence of the quantization of the canonical momentum in a superconductor do not depend on the permeability. Hence, there is the possibility that the ratio between those two fields might be different in a quantum material.

This report summarizes the work carried out in Phase I – the experiment definition, detailed analysis and design. According to the performed analysis, the experimental apparatus described in this report is be able to resolve the gravitational anomaly having an ultimate resolution of 0.3 µg and exceeding the required rotational speeds and angular accelerations.

TABLE OF CONTENT

1 INTRODUCTION

One of the authors (MT) recently published a paper **[Tajmar et al. 2003]**, suggesting for the first time that a reported disagreement between experimental measurements and theoretical predictions for the magnetic field in rotating superconductors **[Tate et al. 1989]** might arise from an anomalous high-order gravitomagnetic contribution (also known as frame dragging or Lense-Thirring effect). In normal matter, the ratio between electromagnetic and gravitational fields is given by the difference in the respective permeabilities. However, magnetic fields generated as a consequence of the quantization of the canonical momentum in a superconductor do not depend on the permeability. Hence, there is the possibility that the ratio between those two fields might be different in a quantum material.

For Tate's experiment, a delta-gravitomagnetic field of at least $\Delta B_g = 1.62 \times 10^{-6}$ rad.s^{-1} would be required to match the theoretical prediction of quantum and relativity theory. This is certainly above any classical coupling phenomena and will be investigated within this research program. Therefore, a facility is designed to rotate a high-temperature superconductive ring and measure, based on the Einstein-Maxwell equations of weak gravitational interactions **[Tajmar et al. 2001]**, induced gravitoelectric fields using highly sensitive accelerometers by varying the speed of rotation. This report summarizes the design of the cryostat and the rotational superconductor assembly, as well as the selection of the major components and test plans to proceed with the actual measurement.

2 EXPERIMENT DEFINITION

2.1 Requirements for Experimental Assembly

Tate et al **[Tate et al. 1990]** followed Ginzburg-Landau theory, integrating the current density of Cooper pairs around a closed path including the effect of a rotating reference frame, but neglecting any gravitomagnetic fields:

$$\frac{m^*}{e^2 n_s} \oint_\Gamma \vec{j} \cdot d\vec{l} = \frac{nh}{2e} - \int_{S_\Gamma} \vec{B} \cdot d\vec{S} - \frac{2m^*}{e} \cdot \vec{\omega} \cdot \vec{S}_\Gamma ,$$ (2.1)

where n_s is the Cooper-electron number density, S_Γ is the area bounded by Γ, ω the angular velocity, B the London moment and m^* the Cooper-pair mass measured by Tate. The argument put forward in **[Tajmar et al. 2003]** says that Tate's measured Cooper-pair mass m^* is different from the theoretically expected one m because Equ. (2.1) does not account for a possibly involved gravitomagnetic field B_g. The complete Ginzburg-Landau equation should read as

$$\frac{m}{e^2 n_s} \oint_\Gamma \vec{j} \cdot d\vec{l} = \frac{nh}{2e} - \int_{S_\Gamma} \vec{B} \cdot d\vec{S} - \frac{m}{e} \int_{S_\Gamma} \vec{B}_g \cdot d\vec{S} - \frac{2m}{e} \cdot \vec{\omega} \cdot \vec{S}_\Gamma .$$ (2.2)

Combining both equations we can express the gravitomagnetic field B_g as

$$\vec{B}_g = 2\vec{\omega} \cdot \left(\frac{m^* - m}{m} \right) + \left(\frac{m^* - m}{m} \right) \cdot \frac{1}{\vec{S} e n_s} \oint_\Gamma \vec{j} \cdot d\vec{l} .$$ (2.3)

In a superconductor that is thick compared to the London penetration depth, the current integral in the above equations can be set to zero as there is always a path inside the superconductor in which no current is flowing (outside the London penetration depth). The gravitomagnetic field is then just a function of the angular velocity and the mass difference of the Cooper-pairs

$$\vec{B}_g = 2\vec{\omega} \cdot \left(\frac{m^* - m}{m} \right). \tag{2.4}$$

For the case of Niobium, based on Tate's measurement, we can expect a gravitomagnetic field according to **Figure 2.1-1**.
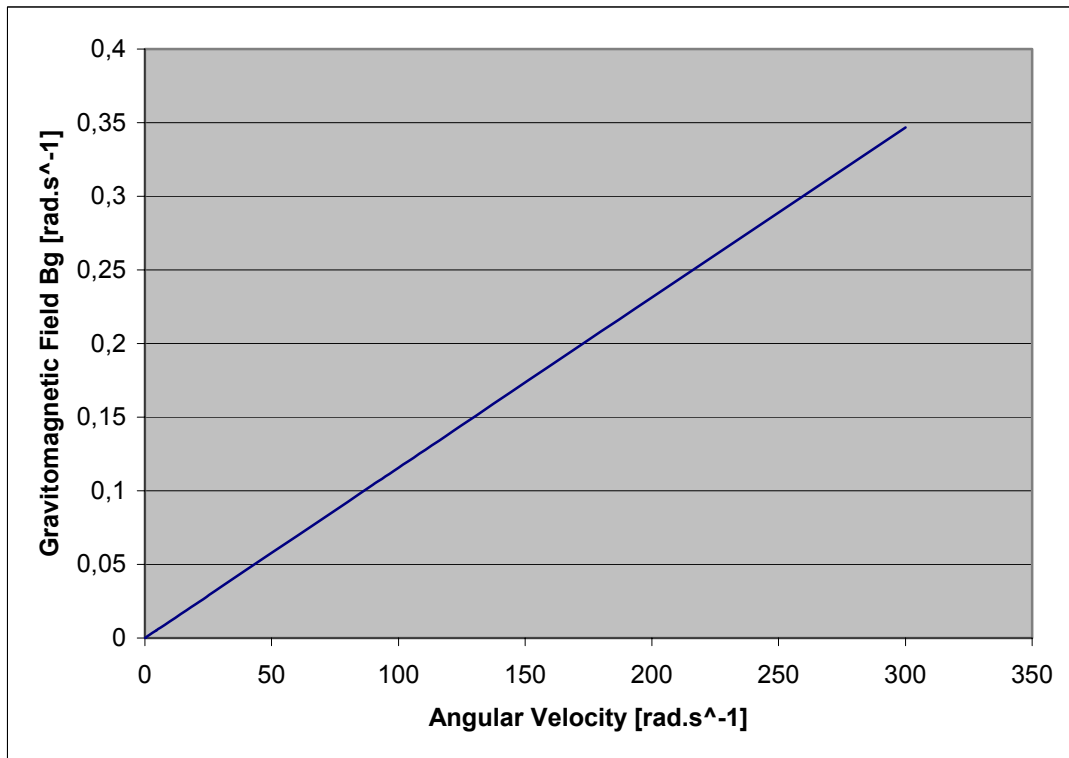
Figure 2.1-1 Expected gravitomagnetic field in thick Niobium superconductor as a function of angular velocity.

As the gravitomagnetic field is related to a gravitational field using the equations given by Tajmar and De Matos ([**De Matos** et al. 2001][**Tajmar** et al. 2001][**Tajmar** et al. 2003]).
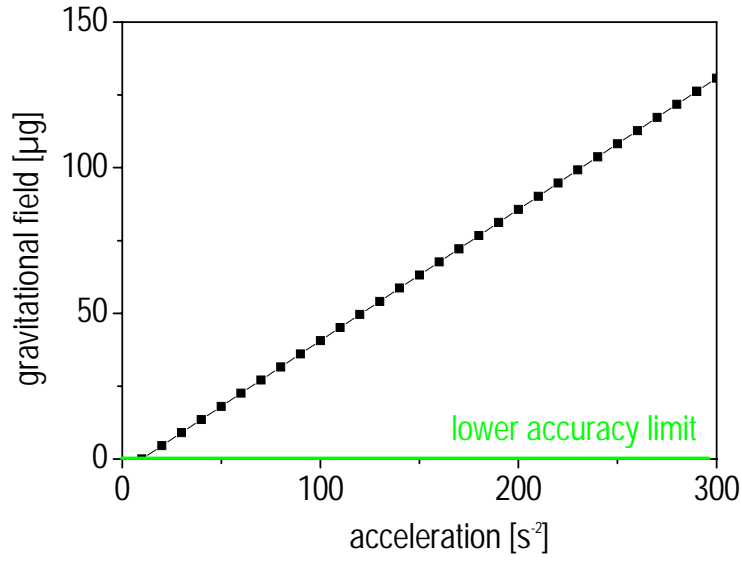
$$\vec{\nabla} \times \vec{g} = -\frac{\partial B_g}{dt} \qquad (2.5)$$

$$\oiint \vec{\nabla} \times \vec{g}\, d\vec{A} = \oint \vec{g}\, d\vec{s} = \oiint -\frac{\partial B_g}{dt}\, d\vec{A} \sim 2r\pi\vec{g}$$

an accelerated superconductor should show a change of the gravitational field. Combining Equ. (2.5) with (2.1), we can express the expected gravitational field at radial position r by

$$\vec{g} = -\dot{\vec{\omega}} \cdot \left(\frac{m^* - m}{m} \right) \cdot \frac{R^2}{r} \, . \qquad (2.6)$$

where R is the outer radius of the superconducting ring. The result is shown in **Figure 2.1-2**.

Figure 2.1-2   Expected gravitational field as a function of superconductor acceleration.

In order to get a measurable signal (assuming a resolution of 1µg of the acceleration sensor - see chapter 2.2.1), the necessary acceleration of the ring can be calculated to be higher than 200 s^{-2}. The distance between the acceleration sensor and the superconducting ring was chosen to be 30 mm in accordance with the design of the experiment. The area of the superconducting ring is 7 x 15 mm² as offered by Nexans superconductors (see chapter 2.2.2).

In order to get reasonable experimental results, the desired acceleration was taken to be 1.5 times the estimated acceleration (note, that one can expect a linear relation between the acceleration and the gravitational field). In order to allow filtering of the signal at the highest achievable acceleration of 300 s^{-2}, this acceleration has to be maintained for at least 1 second, resulting in a maximum rotational speed of 300 s^{-1} corresponding to approximately 3000 rpm.

In order to perform the experiment, the superconductor has to be cooled below its transition temperature. Therefore, a temperature limit of 77 K (LN$_2$) was chosen. However, due to the design of the experiment, an upgrade to 4.2 K (liquid He temperature) is possible without significant changes.

All requirements for the experimental facility are summarized in **Table 1**.

Resolution of Acceleration Sensor	1 µg
Angular Acceleration of Superconductive Ring	> 200 s^{-2}
Minimum Measurement Time	1 s
Maximum Rotational Speed of Superconductive Ring	3000 rpm
Temperature of Superconductive Ring	77 K (LN$_2$)

Table 1 Summary of Requirements for Experimental Facility

2.2 Trade-Off Study for Major Components

2.2.1 Accelerometer and Electronics

There are several demands, which have to be reached by the accelerometer:

1) The accelerometer has to be small enough to fit into the superconducting ring. The measurement area has to be small compared to the inner diameter in order to measure the local acceleration instead of an average.

2) The signal has to be measured inert (without movement of the accelerometer) i.e. accelerometer has to show 1 g when being subjected to earth gravitational field.

3) The resolution of the accelerometer has to be high enough to reach at least 1 µg. For a lower resolution, the acceleration of the SCR has to be increased (see **Figure 2.1-2**), causing several design problems.

4) As there are nine accelerometers necessary (two positions near the surface, and one a referent position, each position consisting of three acceleration axes), also the price is an important factor.

After an extensive survey, four accelerometers have been investigated for their adaptability (all types are hermetically sealed and therefore compatible with vacuum operation) which are summarized in **Table 2** (Note: only the MWS sensor is a three-axis sensor, all other ones are single-axis sensors).

Manufacturer / Product	Resolution	Size	Price
Honeywell QA3000 Q-Flex **[Honeywell]**	50 ngHz$^{-0,5}$	25 x 25 x 25 mm	5500 $/pc
Applied MEMS Si-Flex SF1500ULND **[Applied Mems]**	300 ngHz$^{-0,5}$ low frequency noise ~3 µgHz$^{-0,5}$	63 x 45 x 13 mm	600 $/pc
Silicon designs 1221L-02 **[Silicon Designs]**	2 µgHz$^{-0,5}$ (down to 0,2 Hz)	8 x 8 x 3 mm (including electronics)	200 $/pc
MWS Sensorik BS 5401 (3-axis) **[MWS]**	25 µgHz$^{-0,5}$	23 x 18 x 16 mm	2300 $/pc

Table 2   Accelerometers Investigated for their Adaptability

As the resolution demand is 1 µg with a signal to noise ratio of at least 3 and a signal length of at least 1 s with at least 10 data points (= 10 Hz), the MWS sensor does not reach the demands of resolution. The best performing sensor is obviously the Honeywell Q-flex. But mostly due to its size and its high price, it has to be ruled out at the present stage.

The two remaining sensors (the Silicon Design and the applied MEMS accelerometers), are quite similar in price, however, the applied MEMS one is due to its large electronics (which has to be attached directly on the chip) too big for placing it inside the superconducting ring. Therefore, the Silicon Design 1221L-02 accelerometer (see **Figure 2.2-1**) was selected as the baseline, which has of course some shortcomings in resolution that can be balanced by proper measurement electronics.
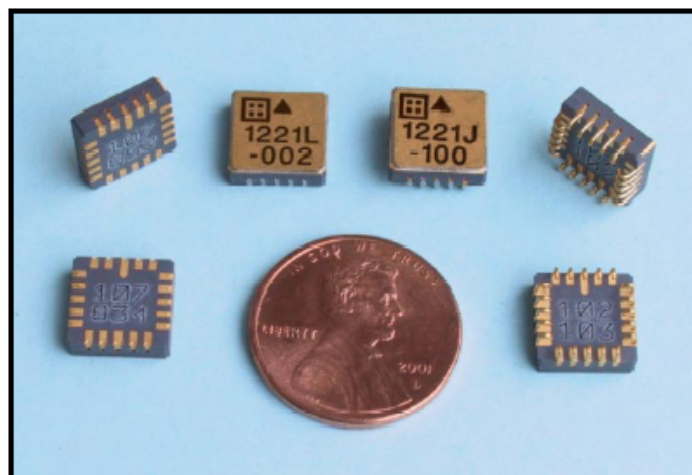

Figure 2.2-1   Photograph taken from the Silicon Designs 1221L-02 chip.

Silicon Design's accelerometers use capacitance change due to acceleration force as the sensed parameter. A capacitive approach allows several benefits when compared to the piezoresistive sensors used in many other accelerometers. In general, gaseous dielectric capacitors are relatively insensitive to temperature. Although spacings change with temperature due to thermal expansion, the low thermal coefficient of expansion of many materials can produce a thermal coefficient of capacitance about two orders of magnitude less than the thermal coefficient of resistivity of doped silicon. Therefore, the demands on the temperature regulation system can be kept minimal.

As compared with piezoelectric type accelerometers which require a dynamic input of some minimum frequency to generate a response, a capacitive sensing allows for response to DC accelerations guaranteeing a fully inert measurement.

Silicon Design's basic accelerometer unit is a 20 pin LCC package containing two parts: the Sense Element or sensor chip and the integrated electronics or ASIC chip **Figure 2.2-2**.
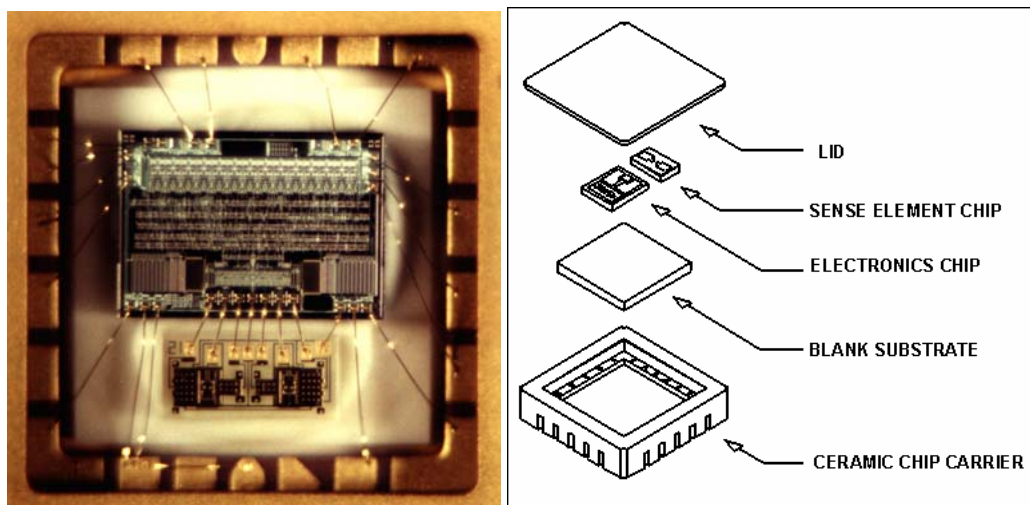
Figure 2.2-2   Photograph of the interior of the chip (left) and exploded schematic drawing (right).

The basic structure of the SDI sense element is shown below. The sense element wing is a flat plate of nickel supported above the substrate surface by two torsion bars attached to a central pedestal. The structure is asymmetrically shaped so that one side is heavier than the other, resulting in a center of mass that is offset from the axis of the torsion bars. When an acceleration force produces a moment around the torsion bar axis, the plate or wing is free to rotate, constrained only by the spring constant of the torsion bars.

On the substrate surface, beneath the sense element wing, two conductive capacitor plates are symmetrically located on each side of the torsion bar axis. The upper wing and the two lower capacitor plates on the substrate form two air-gap variable capacitors with a common connection. This creates a fully active capacitance bridge. When the wing rotates about the torsion bar axis, the average distance

between the wing and one surface plate decreases, increasing the capacitance for that plate, while the distance to the other plate increases, decreasing its capacitance (see **Figure 2.2-3**) .
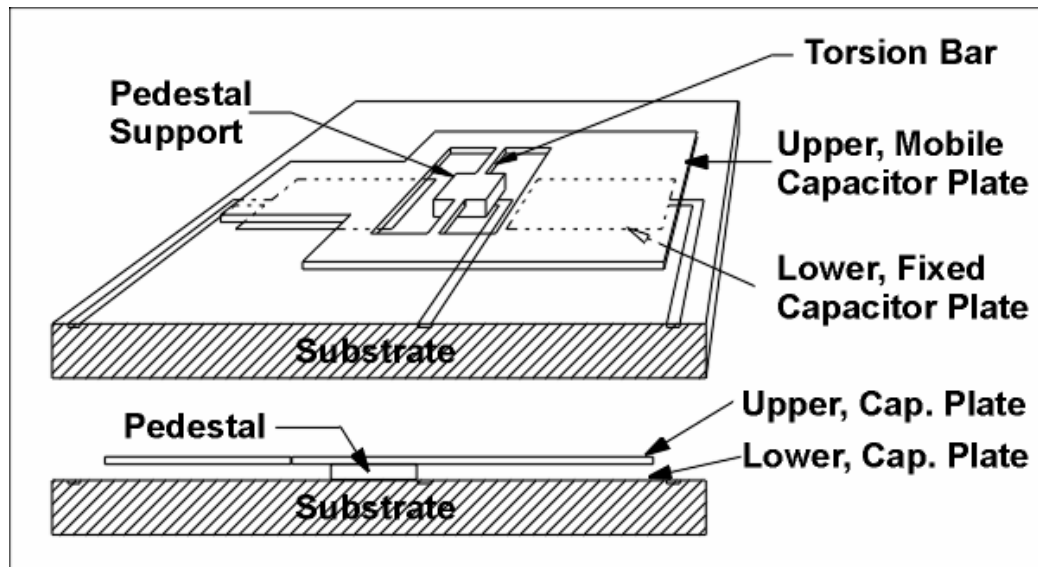

Figure 2.2-3   Operational principle of the accelerometer.

The sense element wings are approximately 1000 microns long by 600 microns wide and 5 to 10 microns thick. The wing to substrate spacing of about 5 microns results in a capacitance from the wing to each lower plate of about 0.15 pF.   The sensitivity of the sense elements (the ratio of deflection to acceleration) is determined by the mass of the sense element, the distance from the center of mass to the torsion bar axis, and the torsion bar stiffness. Each complete sense element chip contains two wings for a total of four sensing capacitors.

The output of the Silicon Design's chip is a differential voltage of ± 2 V (at full scale of ± 2g), making it necessary to measure voltages as low as 2 μV with a resolution of at least 100 nV. Therefore, a Keithley Nanovoltmeter 2182 (a two channel Voltmeter with a resolution of 10nV/100 nV for Channels one/two) has been chosen. The nanovoltmeter comes with an integrating A/D converter (the integration time can be adjusted in terms of 0.2 ms) and a digital moving filter (for the details of this filtering, we refer to the manual **[Keithley]**). The output can be red from an analog 0-10 V channel or directly using the GBIP interface. Full control of the nanovoltmeters can be taken from the computer using SCIP

protocol. Therefore, this part of the experiment can be remotely controlled avoiding human movements and subsequently vibrations in the vicinity of the experiment.

A simulated signal of 1 µg calculated for the Silicon designs 1221L-02 accelerometer attached to a 10 Hz lowpass filter and acquired by the Keithley 2182 nanovoltmeter with integration time of 20 ms (=1 Power-Load-Cycle PLC) and a digital moving filter of 10 is shown in the upper **Figure 2.2-4**. The Keithley settings are changed to 2 PLC and digital moving filter of 50 for the 0.3 µg signal shown in **Figure 2.2-4**.
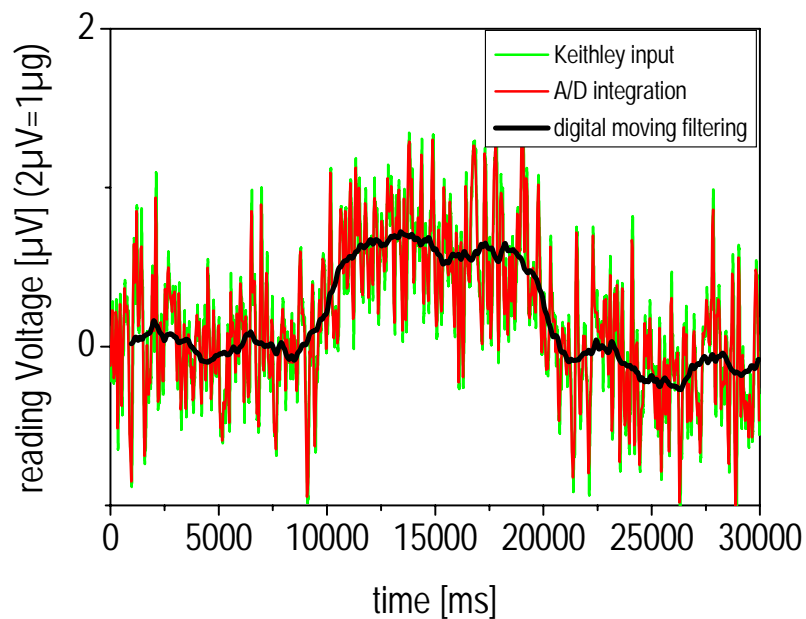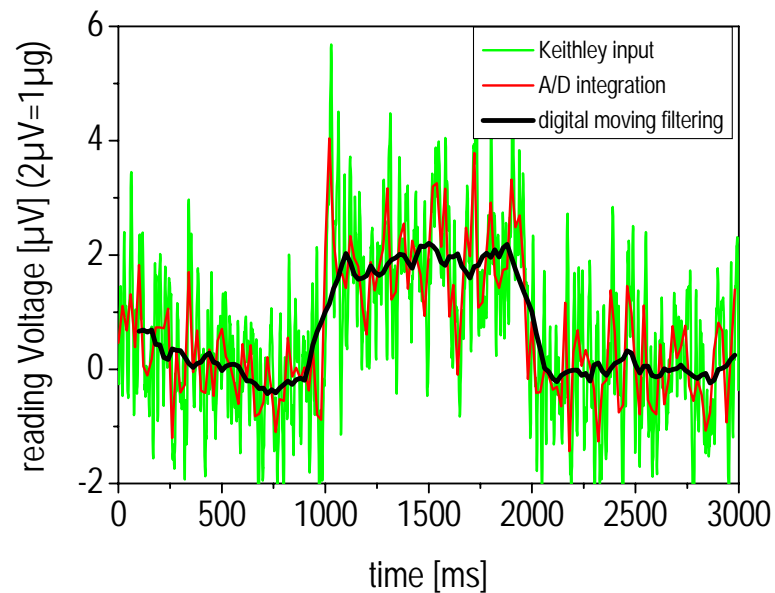
Figure 2.2-4 Simulated Signal of the Acceleration Sensor (upper: 1µg signal; lower: 0.3 µg signal). The green line gives the sensor output filtered using a 10 Hz low pass filter. The black line is the reading of the Keithley nanovoltmeter after integration time of 0.5 or 2 PLC (digital moving filter disabled). Enabling the digital moving filter with a filter count of 10 or 50, results in the red signals. The signal noise ratio is better than 3 for both signals.

2.2.2 Superconductor

Two types of high-temperature superconductors (HTC) are commercially available:

1) <u>YBCO</u>: The material is grown as multi domain structure. Three suppliers have been contacted:

Nexans superconductors: The production of the ring can be done either with glued segments or directly using a 12 domain ring (12 seeds crystals are necessary). The orientation of the grains will be axial. Therefore the superconducting plane will be the radial plane. However, the grain boundaries at the segment interfaces can serve as Josephson junctions. The success of producing such a ring can not be guaranteed. The price for a trial was quoted at 6730 €.

ISTEC: The International Superconductivity Technology Centre is world leader in producing large superconducting bulk-devices. A production of a single domain ring could be possible. However the properties will decay towards the edges of the disk. Therefore, a single domain ring with good properties can not be guarantied. A price can not be quoted so far, but will be higher than the Nexans Superconductors product.

CAN Superconductors: The largest standard disk has a diameter of 50 mm (far from the experimental design). A try for a bigger multi seeded ring was roughly estimated to be in the order of 10 k€.

2) <u>BSCCO</u>: The Material can be produced as long conduit and will be aligned by melt-texturing. **Nexan superconductor** offered a standard BSCCO ring with an outer diameter of 150 mm and 6 mm wall thickness with a height of 15 mm for 1380 € (a higher ring is possible). For a ring with 15 mm wall thickness, the costs will be 3240 €, but the success can not be guaranteed due to the problems of the melt texturing process for such wall thicknesses.

American Superconductors, SCI Engineered Materials and the Slovakian Academy of Sciences (Group of P. Kovac and M. Polak) noted that they are only producing tape material, and are not producing bulk materials. The Austrian leader in superconductivity (Prof. Harald Weber from the Atomic Institute of the Vienna University of Technology) referred to contact ISTEC.

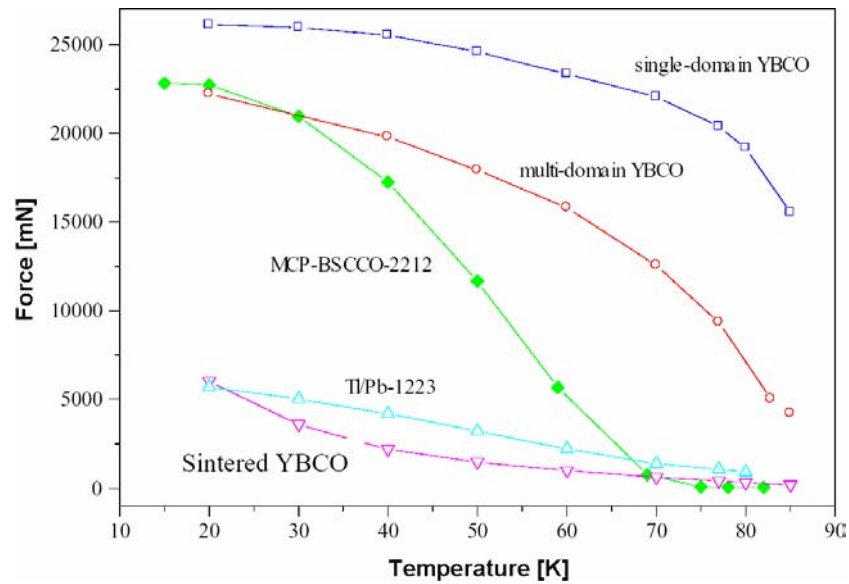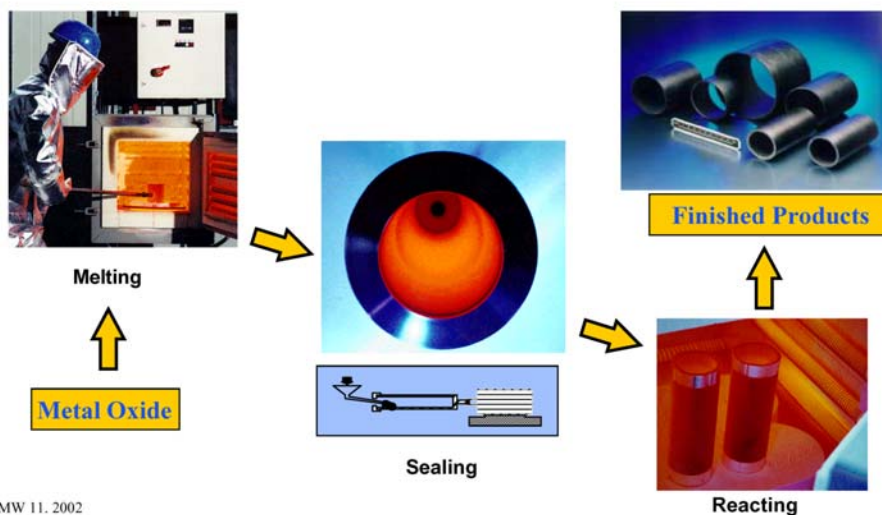Therefore, the BSCCO ring offered by NEXANS superconductors was selected.

Figure 2.2-5   Levitation Force of Different Superconducting Materials as a Function of Temperature

Figure 2.2-6   Production Process of BSCCO Melt Textured Material

Production of Multi-Seeded YCBO Rings

**Preparation Steps YBCO-Ring with 9 Domains d_a= 100 mm**

| Sintered Ring Produced at Nexans, drilled | Seeds Embedded Holes Filled | Textured Ring | Finished Ring |

BMW 11. 2002

Figure 2.2-7 Production Process of YBCO Multi Seeded Ring

2.2.3 Motor Assembly

As motor, a brushless servo motor with computer controllable amplifier (ability of remote control of the experiment) was chosen. The rotational speed, as well as the acceleration given in **Table 1** has to be reached by the motor. Obviously, there are several motors reaching the demands. As all motors are similar in performance and price, it was decided to take the motor from Torque Systems (an American supplier) **[Torquesystems]**. For the amplifier, the PWM Brushless Sinusoidal Servo amplifier was chosen. The amplifier allows for full control of the rotational speed or the applied torque and allows running step less profiles.

As the moment of inertia of the rotating part in the experiment (superconductor including the support structure) has a designed value of 0.010 kgm², the torque necessary to reach 300 s^{-2} is 3 Nm. Therefore, the BNR3034 brushless servo motor was chosen. This motor is fully compatible with the servo amplifier, and allows for a maximum stall torque of 3.8 Nm (a peak torque of 16.95 Nm), as well as a maximum operation speed of 5800 rpm. Therefore, the design goals are completely reached, and can even be extended without changing the motor setup (the mechanical stability to do so have to be checked during the evaluation phase). The weight of 4.3 Kg has to be carried by the structure. The moment of inertia of the rotor is about 10 % of the moment of inertia of the experimental structure, and does therefore not significant effect the performance of the motor.
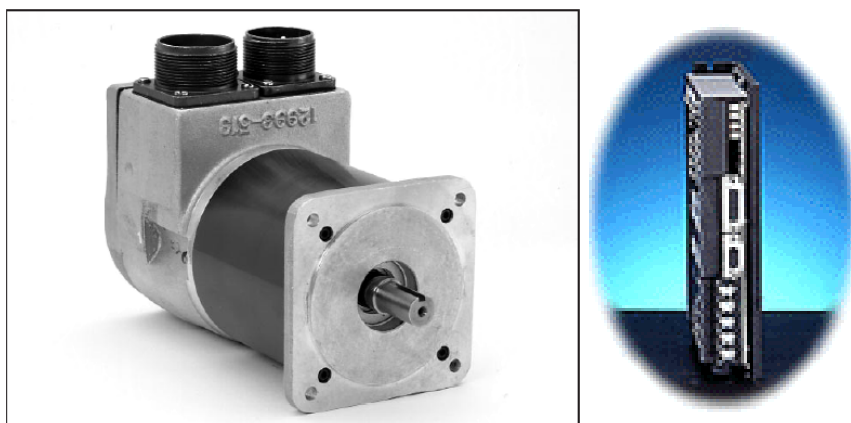
Figure 2.2-8 Motor and Servo Amplifier Proposed to be Used in the Experiment

In order to estimate the influence of the magnetic field acting on the superconductor due to the motor at maximum acceleration, the motor windings can be approximated as a simple coil pointing toward the superconductor. No shielding of the magnetic field due to the cryostat structure etc. is assumed. It has to be emphasized, that this situation shown in **Figure 2.2-9** is a clear overestimation of the actual situation.
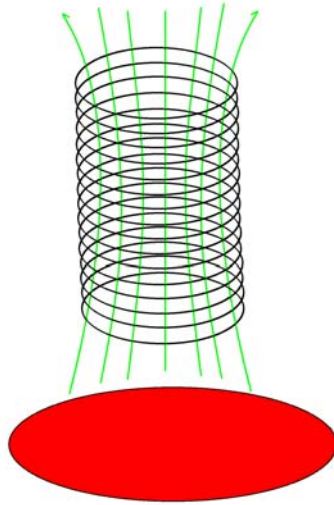
Figure 2.2-9   Schematic sketch describing the magnetic field due to the motor acting on the superconductor.

By using

$$L = \frac{N^2 \mu_0 A}{l} \tag{2.2}$$

$$B = \mu_0 I \frac{N}{l} \frac{A}{4\pi} \left(\frac{1}{\left(d - \frac{l}{2}\right)^2} - \frac{1}{\left(d + \frac{l}{2}\right)^2} \right)$$

one can calculate the magnetic field to be

$$B = I \sqrt{\frac{LA\mu_0}{l}} \frac{1}{4\pi} \left(\frac{1}{\left(d - \frac{l}{2}\right)^2} - \frac{1}{\left(d + \frac{l}{2}\right)^2} \right) \tag{2.3}$$

The current I=6.6 A (for a torque of 3.8 Nm at a rate of 0,57Nm/A). The inductance L=4.9 mH. The dimensions of the motor (area A and length l) have been estimated to be about 60 % of the outer dimensions of the motor. The distance z from the motor to the superconductor has been estimated from the design drawings to be 400 mm. Taking all this data as an input to equation (2.3), the magnetic field coming from the motor is about 30 µT, and is therefore in the same order of magnitude as the earth magnetic field (30-60 µT). As the described situation is definitely an overestimation of the actual situation, the magnetic influence of the motor can be neglected.

Air motors (having no magnetic moment acting on the superconductor) are ruled out, as their control is much more complicated compared to standard servo motors, and high torques and high rotational speed are not easily achievable. Products supplied from Duesterloh, Dynatork, Kinequip and PSIautomation have been investigated **[Airmotors]**.

3 EXPERIMENT DESIGN

3.1 Overview of Complete Assembly

The interplay and principal assembly of the key-components described above is shown in the block diagram in **Figure 3.1-1**. In addition to the key components, a temperature regulation for some parts is necessary to maintain the operational condition of these components.
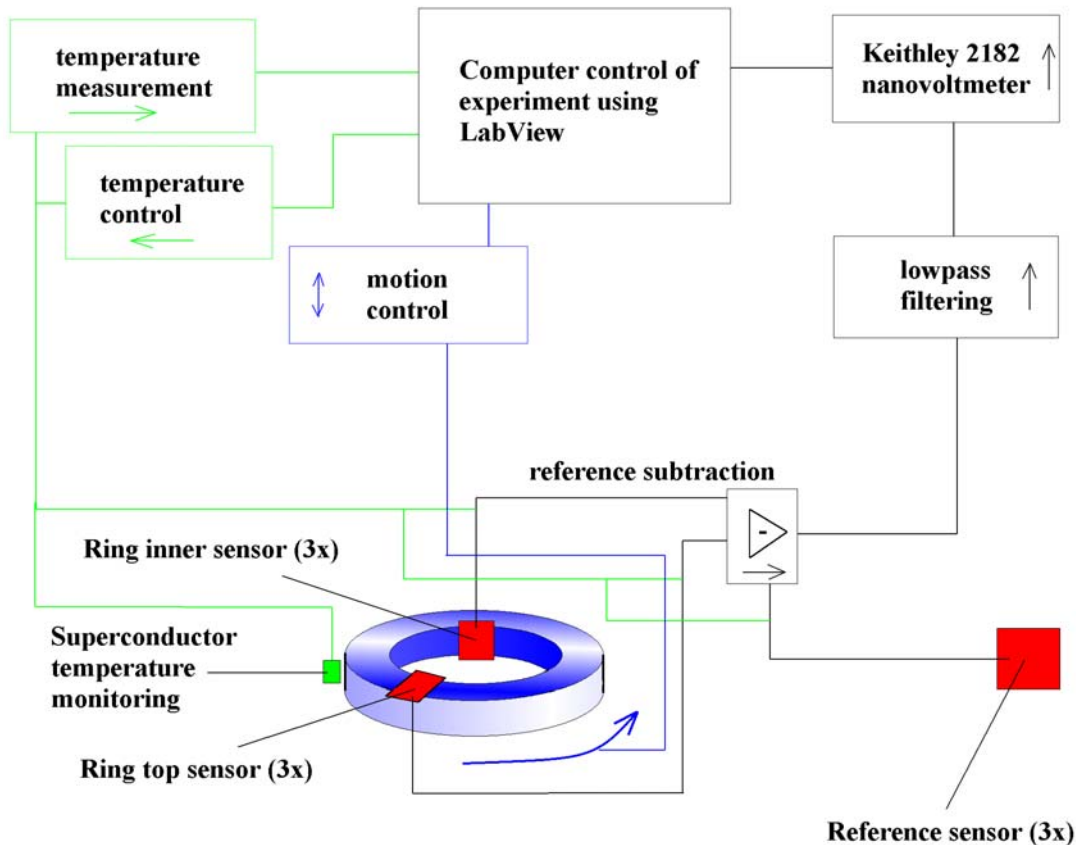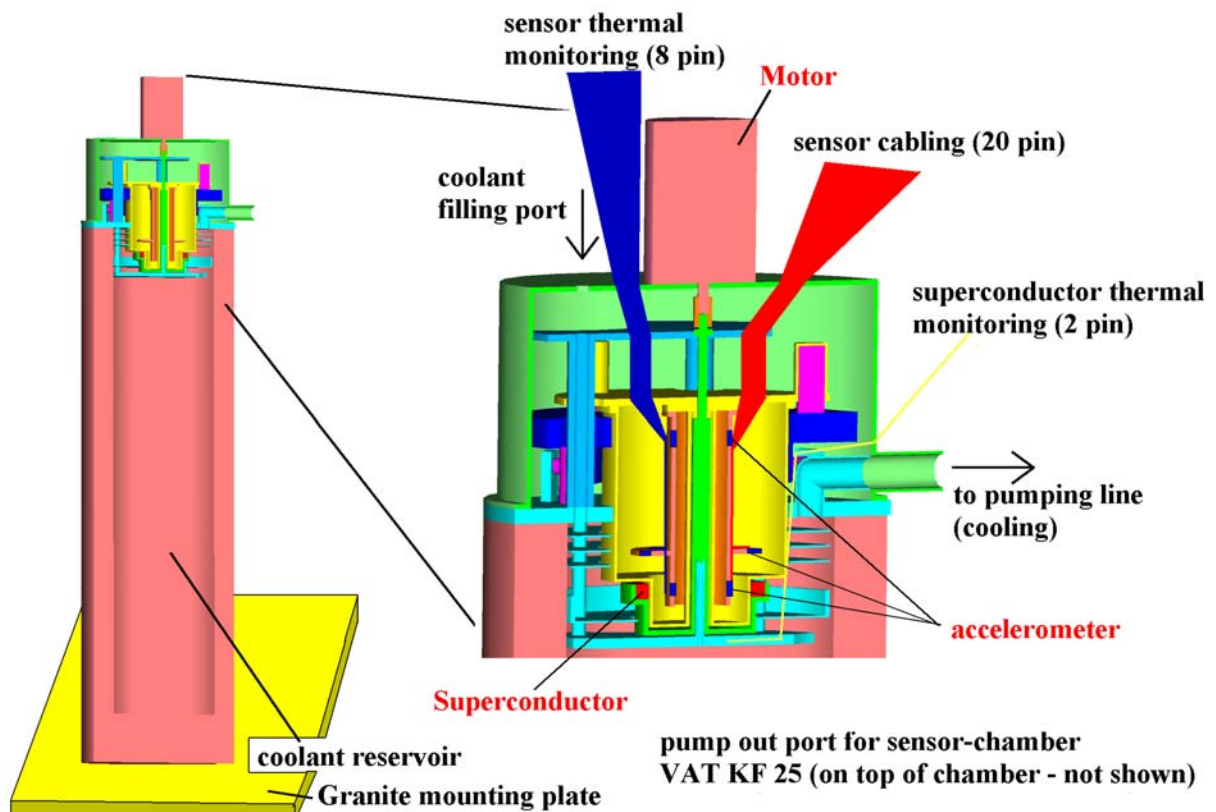

Figure 3.1-1 Block Diagram of the Experimental Setup

The design of the experiment identifying the key components and the information flow path shown in **Figure 3.1-1** is given in **Figure 3.1-2**.

Figure 3.1-2 Design of the Experiment identifying the Key Components and the Information Flow Path

The detailed design identifying the structural elements of the experiment is shown in **Figure 3.1-3**. The cryogenic system is omitted in this figure.
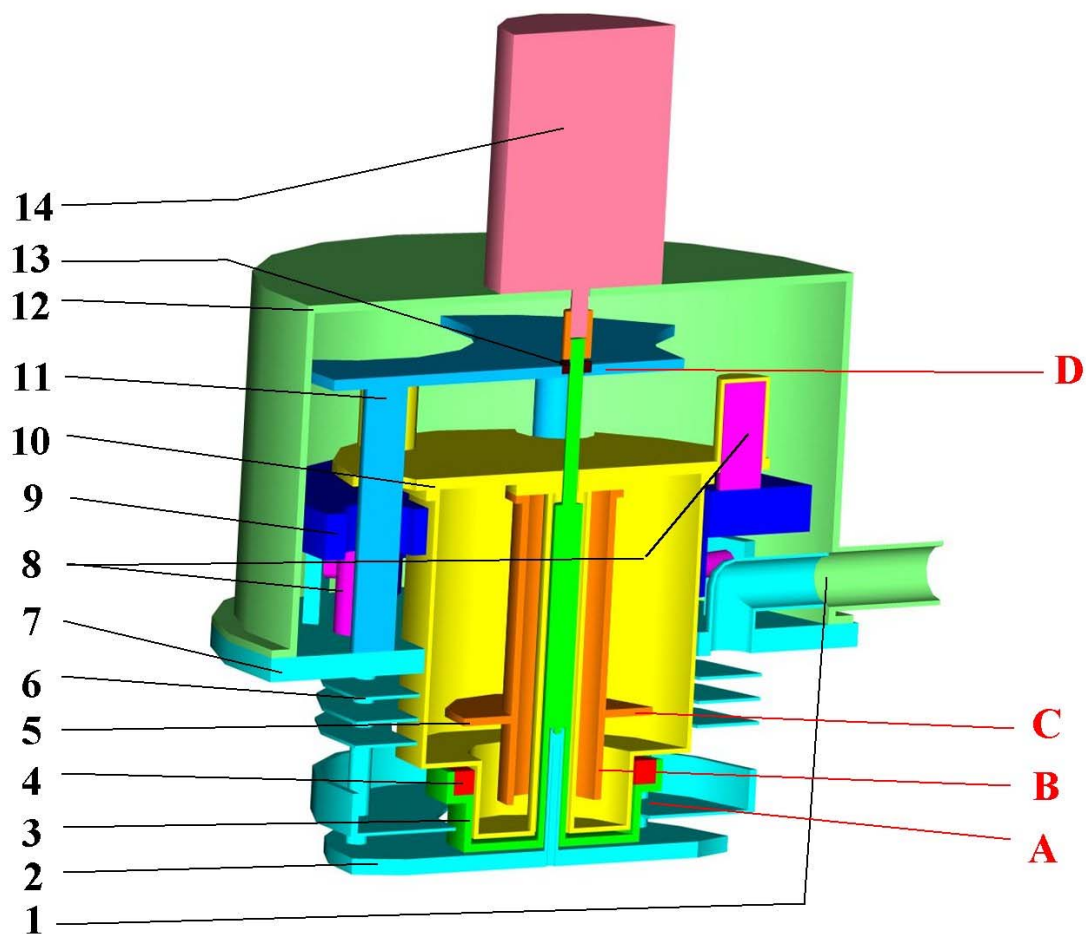
Figure 3.1-3   Complete Design of the Experiment. The black numbers mark structural design parts. The red letters state temperature measurement and –regulation points. As this is only the design, for the detailed solutions (including cryostat, cabling and valves) see later.

1) Coolant exhaust port. The conduit coming out of part 7 is used to prevent the upper parts from being extensively cooled by cryogenic gas.

2) Lower support structure for the rotating part. The cold bearing is designed to be radial ball bearing with solid lubricant.

3) Support structure for the superconducting ring. The support structure carries the SCR, and is attached directly to the Motor (Part 14)

4) Superconducting ring

5) Mounting structure for the accelerometers and Gauss-meter

6) Radiation shields (thermal design). The radiation shield at the height of the SCR acts as structural support for the magnetic field coil #5, as well as as coolant guide force the gas flow toward the SCR support structure.

7) Mounting flange. The whole structure is connected via the mounting flange to the cryostat (the cryostat is not shown in the design).

8) Vibrational damping springs. The operation will be explained in much detail in the following sections.

9) First stage ring of the vibrational damping system.

10) Vacuum container carrying the thermal as well as the structural support to allow the operation of the sensors.

11) Upper support structure of the rotating parts. The liquid gas will be supplied through the stilts. This should again prevent extensive cooling of the upper parts especially shortly after the cooling down phases.

12) Experiment closure. In order to prevent cryo pumping of air and humidity to the experimental structure causing the risk of freezing the bearings.

13) Upper bearing (ball bearing)

14) Motor

A) Measurement of the SC temperature. The temperature will be measured about one mm below the lower support structure. Due to the experience given in **[Hense 2002]**; **[Hense 2004]**, the temperature accuracy necessary to control the SCR temperature can be achieved in gas flow regime even when not attaching the thermometer directly to the structure of which the temperature is of interest. In addition, the temperature should have only a minor influence on the effect (even if the temperature is wrong by some tenth of a Kelvin, the influence can be neglected), as long as the superconductor is cooled below its transition temperature.

B) Measurement and Control of the accelerometer temperature in order to achieve the specified temperature range of the SD1221L-02.

C) Measurement and Control of the accelerometer temperature in order to achieve the specified temperature range of the SD1221L-02.

D) Measurement and control of the temperature of the upper bearing in order to prevent freezing of the bearing due to thermal conductivity of the rotating support structure.
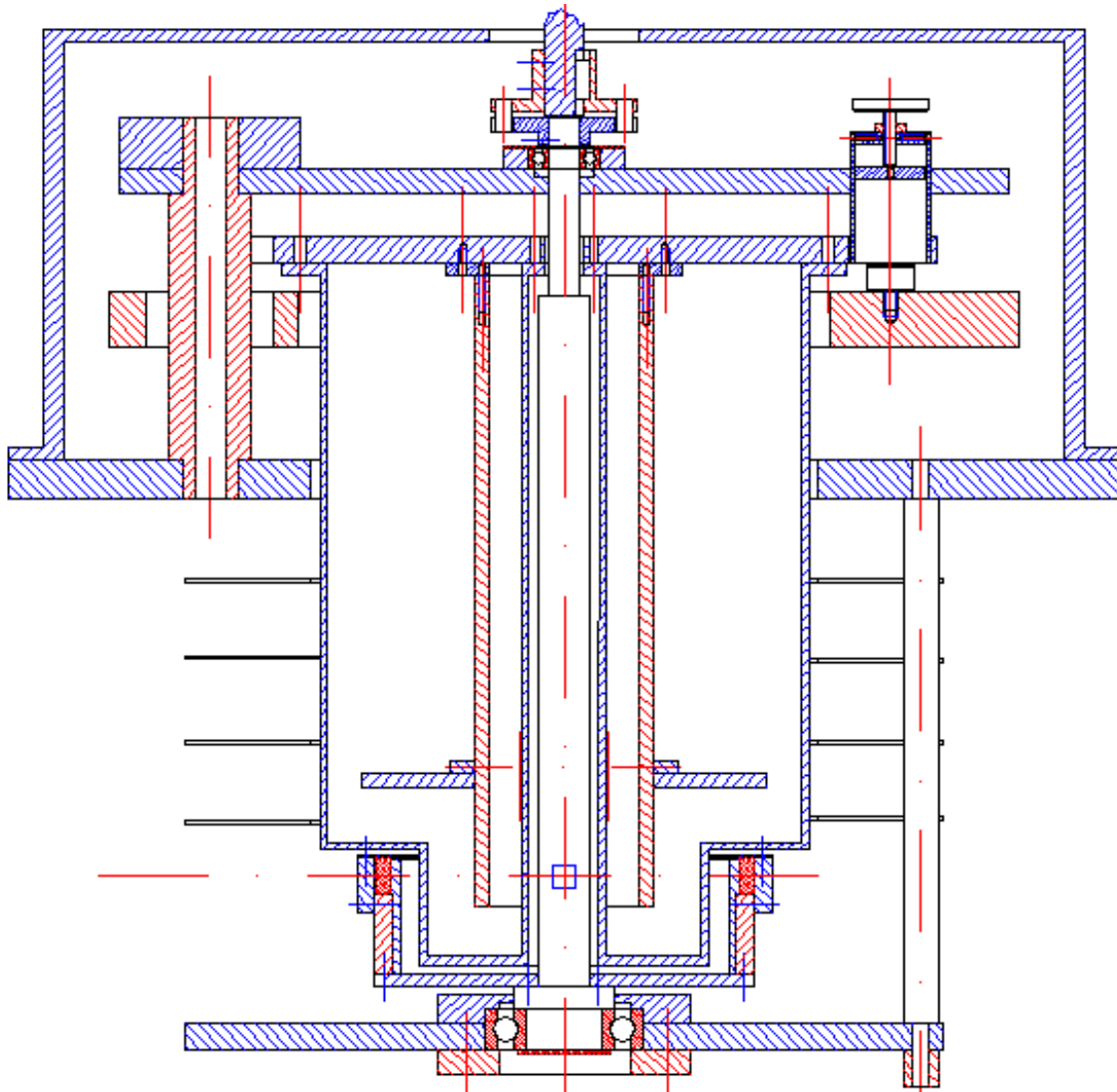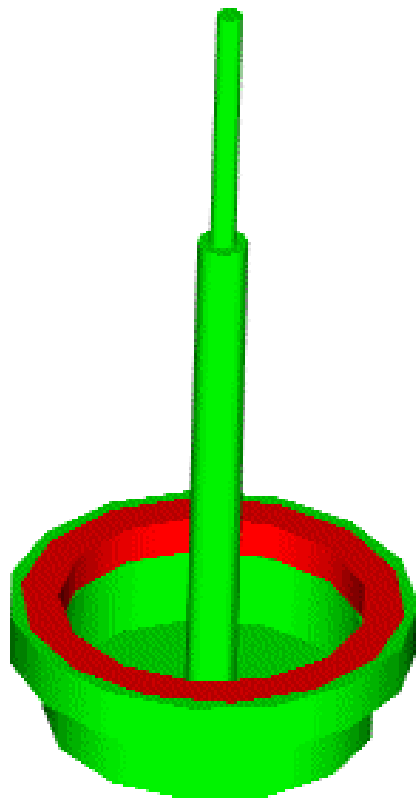
Figure 3.1-4 Mechanical drawing (The drawing is simplified in order to avoid confusions).

3.2 Mechanical Design

3.2.1 Rotational part

The design of the rotating parts (3 and 4 in **Figure 3.1-3**) is shown in **Figure 3.2-1**. The final weight of the rotor is 4 kg, an it's moment of inertia is 0.01 kgm².

Figure 3.2-1 Design of the Rotational Part of the Experiment (Including the Superconducting Ring – Red Color)

In the final construction, the part has to be separated in two functional groups:

1) The lower part of the support structure (which is well separated from the SCR) and the axis going to the motor. This part has to have high mechanical strength (the whole torque will be conducted through this axis), as well as low thermal conductivity in order to prevent heating of the superconductor via the

structure and cooling of the ball bearing at the upper side. The acceleration of the SCR causes a shear stress of about 30 N/mm² (well below the usual upper limit for the torque of 80 N/mm²) in the axes, as well as a torque of 0.5° **[Böge 1989]**.

The upper bearing is a radial roller bearing of type 6001 (axis diameter 12 mm), the inner ring is allowed to move along the axis. The outer ring is fixed in the mounting structure. The connection to the motor is done using a positive fit clutch (see **Figure 3.2-2**).

The lower bearing is a KOYO radial ball bearing, compatible with cryogenic temperatures, with solid lubricant (silver), of 6206 type. The maximal allowed rotational speed of the bearing is specified to be ~3000 rpm. The dynamic load rating of this type of bearing is 1.5 kN (and 75 0N static). The maximal axial force is about 50 N (the weight of the rotor), and the radial force is about 170 N (from the asymmetric rotating superconductor due to imperfect centering caused by thermal expansion). This results in an dynamic equivalent bearing load of 170 N. Using this as an input, the bearing lifetime (assuming the bearing to be operated at 3000 rpm for the whole lifetime) can be estimated to be higher than 4000 h. Therefore, the allowed parameters of the bearing are well within the expected forces acting on it. It has to be emphasized, that this calculation is only necessary for the cold bearing, as the mechanical strength of the standard bearing used on the warm side is 13 times higher than for the same EXCEF bearing (see **Figure 3.2-3**).

For both, the warm and the cold bearing an emergency friction type bearing with a thickness of ~5 mm steel is included, in order to reduce the risk of damaging the experiment in the case of a failure of the roller bearings.
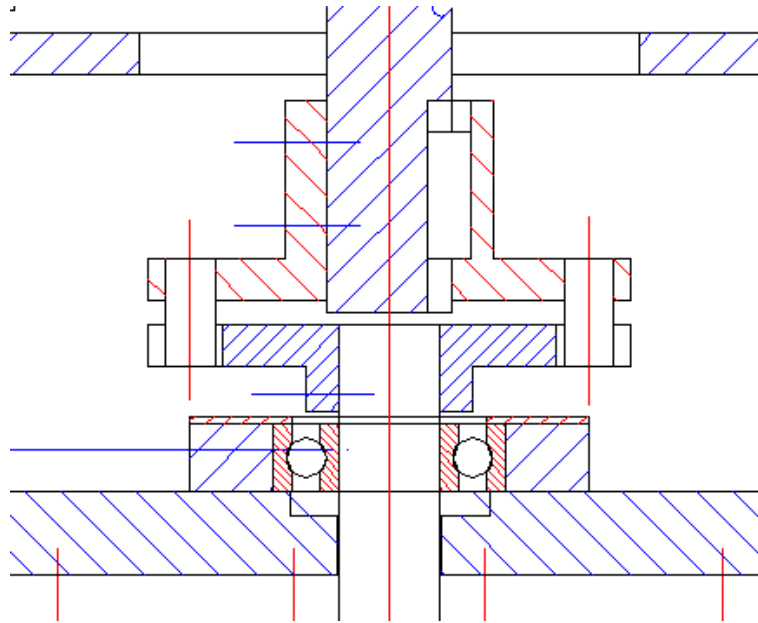
Figure 3.2-2 Clutch between the rotor and the motor. The radial roller bearing is of 6001 type.
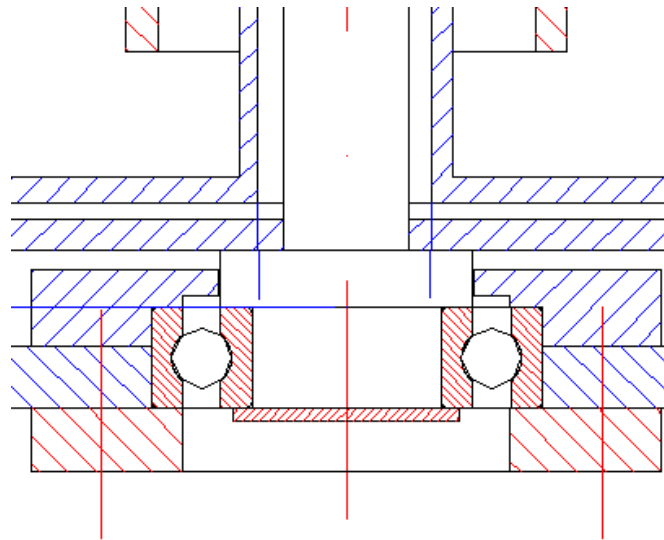
Figure 3.2-3 Design of the cold bearing. The torque is supplied to the support structure using three 3mm bolts separated by 120° from each other).

2) The part supporting the superconducting ring directly. This part should have good thermal conductivity in order to allow a good cooling from the gas flow which passes below the support structure. In order to reduce the moment of inertia due to heavy weight at high radii, this support material has to be pure aluminum. The thermal conductivity of aluminum is 229 W/m K. In comparison,

the thermal conductivity of copper is 372 W/m K, however, the density is 8960 kg/m³ (compared to 2700 kg/m³ for aluminum). The thermal conductivity of steel is typically 16.3 W/m K with an typical density (Steel 1.4301) of 7900 kg/m³ **[VDI1997]**.

The centering of the BSCCO superconductor is done from the inner side (at room temperature), and at cryogenic temperature, the ring is kept in position from the outer side by an aluminum cage, which has three small contacts to the superconductor. This is necessary, as the linear thermal expansion coefficient of BSCCO is about 5.9×10^{-6} K^{-1} in the range down to 10 K **[Escher et al. 1996]**.

The thermal expansion of aluminum in the same range is about 20×10^{-6} K^{-1} **[VDI1997]**. Therefore, the excess contraction of the support structure is about 0.6 mm with respect to the (brittle) HTC superconducting ring. The support structure is designed to center the ring properly at cryogenic temperatures.

In order to prevent the ring from slipping with respect to the support structure, a axial force is applied, to produce frictional connection of the ring to the support structure (see **Figure 3.2-4**).
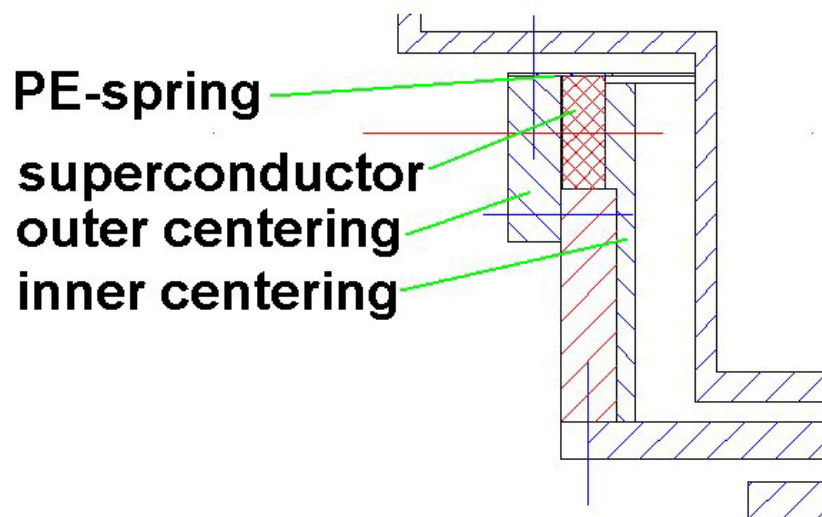

Figure 3.2-4 Centering and frictional connection of the ring to the support structure.

### 3.2.2   Vibrational Isolation of the Accelerometers

The sensors will be put in a separate vacuum chamber, and are packed by a multilayer insulation to maintain the permitted operational temperature of the sensors. This chamber is mounted on a two step vibration isolation system consisting of commercial springs, as well as a copper ring and the vacuum chamber itself as oscillator masses. The setup is shown in **Figure 3.2-5**.
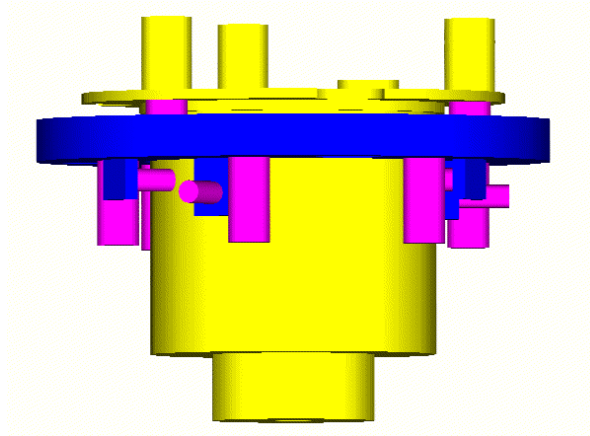
Figure 3.2-5   Sketch of the Vibration Isolation. The springs are plotted violet, mass 1 is given by the blue ring, the yellow ring contains the vacuum chamber with the accelerometers, and serves as second mass. The support structure is not shown in this figure.

The isolation system can be interpreted as a double pendulum as shown in **Figure 3.2-6**. For an elaborated discussion in the analysis of vibrational spectra we referee to the literature **[Hense 1999/2002]**.

Mass M_0 is driven to oscillate by an external force F_0. This force comes from the eccentricity of the rotated superconductor, which is transmitted to the housing (M_0), and from oscillations of the whole system due vibrations of the surroundings (moving persons, traffic, …). The oscillations are transported to mass M_1 (#10) via spring c_1 (#9) and from there to the sensor housing (#11) via spring c_2 (#9). Spring c_0 gives the mounting of the whole structure to the laboratory floor, and is used to isolate vibrations from the surrounding.
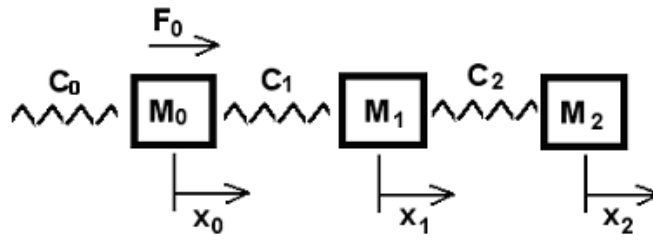
Figure 3.2-6 Schematic Interpretation of the Vibration Isolation System.

Therefore, the equation of motion for this system reads as:

$$M_0 x_0^{//} = F_0 + c_1(x_1 - x_0)$$

$$M_1 x_1^{//} = c_1(x_0 - x_1) + c_2(x_2 - x_1)$$

$$M_2 x_2^{//} = c_2(x_1 - x_2)$$

(3.2)

or alternatively

$$\vec{X}'' = \vec{\vec{C}}\vec{X} + \frac{1}{M_1}\vec{F}_0$$

(3.3)

with the abbreviations

$$M_i x_i = X_i$$

$$\vec{C} = \begin{pmatrix} -\dfrac{c_1 + c_0}{M_0} & \dfrac{c_1}{M_0} & 0 \\ \dfrac{c_1}{M_1} & \dfrac{-(c_1 + c_2)}{M_1} & \dfrac{c_2}{M_1} \\ 0 & \dfrac{c_2}{M_2} & \dfrac{-c_2}{M_2} \end{pmatrix}$$

$$\vec{F}_0 = F_0 \begin{pmatrix} 1 \\ 0 \\ 0 \end{pmatrix} = f_0 \exp(i\omega t) \begin{pmatrix} 1 \\ 0 \\ 0 \end{pmatrix}$$

Assuming harmonic excitations, the oscillations X_i have to be of harmonic type, therefore, the three dimensional linear differential equation can be transformed to a linear equation:

$$X_i = \Psi_i \exp[i(\omega t + \varphi)] = \Psi_i \exp[i\omega t]\exp(i\varphi) = \Theta_i \exp[i\omega t] \tag{3.4}$$
$$X_i^{//} = -\Psi_i \omega^2 \exp[i(\omega t + \varphi)] = -\Theta_i \omega^2 \exp[i\omega t]$$

Note, that the quantity Θ_i is now complex defined. Therefore, a homogenous solution of the problem is defined to be:

$$-\omega^2 \Theta_i = C_{ij}\Theta_j \tag{3.5}$$

Obviously, the above equation has three independent eigenvectors, and three orthonormal eigenvectors. Therefore, the matrix C_{ij} can be transformed to diagonal form using

$$\left(\vec{\Theta}^T\right)_{im} C_{ml} \vec{\Theta}_{lj} = \omega_i^2 \delta_{ij} \tag{3.6}$$

Note, that on the right hand side of above equation, the Einstein convention must not be applied. The notation simply represents a diagonal matrix, where the diagonal elements are the eigenfrequencies ω_i. Applying above transformation to the inhomogeneous equation, one ends up with

$$\Phi_i'' = \left(\ddot{\Theta}^T \ddot{C} \ddot{\Theta}\right)_{ij} \Phi_j + \left(\ddot{\Theta}^T\right)_{ij} \left(F_0\right)_j = \omega_i^2 \delta_{ij} \Phi_j + \gamma_i \tag{3.7}$$

where the Φ_i's are the normal modes of the system. As the matrix $\left(\ddot{\Theta}^T \ddot{C} \ddot{\Theta}\right)$ is now diagonal, the three equations are decoupled, and therefore, the system can be treated as three (independent) driven oscillators, with the well known solutions

$$\Phi_i = \frac{\gamma_i}{M_0} \frac{1}{\omega_i^2 - \omega^2} \tag{3.8}$$

which can be transformed back to the coordinates X_i using the matrix $\ddot{\Theta}$. Therefore, one ends up with (including a damping δ)

$$X_i = \Theta_{ij} \frac{\gamma_j}{M_0} \frac{1}{\sqrt{\left(\omega_j^2 - \omega^2\right) + 4\delta^2 \omega^2}} \exp(i\omega_j t) \tag{3.9}$$

In the present case, not the amplitude of the oscillations transferred through the isolation system are of interest, but only the accelerations acting on the accelerometers, which are the second derivative of X_3. Assuming the driving force to come from the rotating superconductor, the driving force can be assumed to be:

$$F_0 = m\, r_{ex}\, \omega^2 \tag{3.10}$$

where m is the mass that is rotational asymmetric, and r_{ex} is the radius of this asymmetry (the displacement of the centre of gravity from the ideal axis).

For the further analysis, it is obvious that the eigenfreuquencies of the system have to be as low as possible. Therefore, the dependence of the eigenfrequency as a function of the input parameter was done putting above equations to Mathematica by Wolfram research. The results are shown in **Figure 3.2-7** and **Figure 3.2-8**.
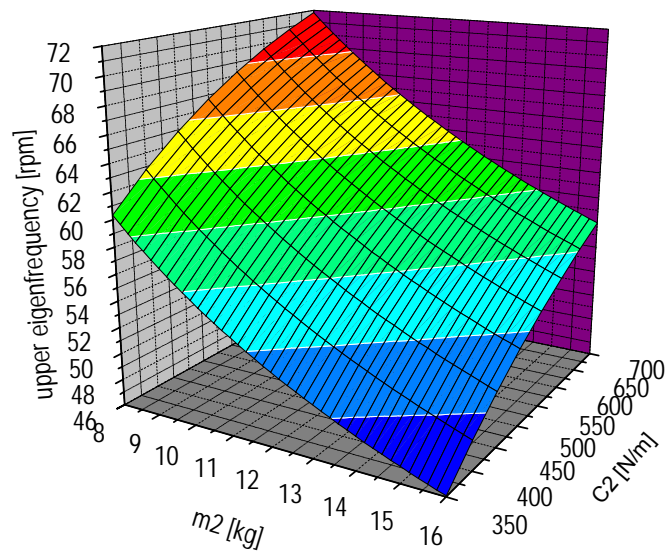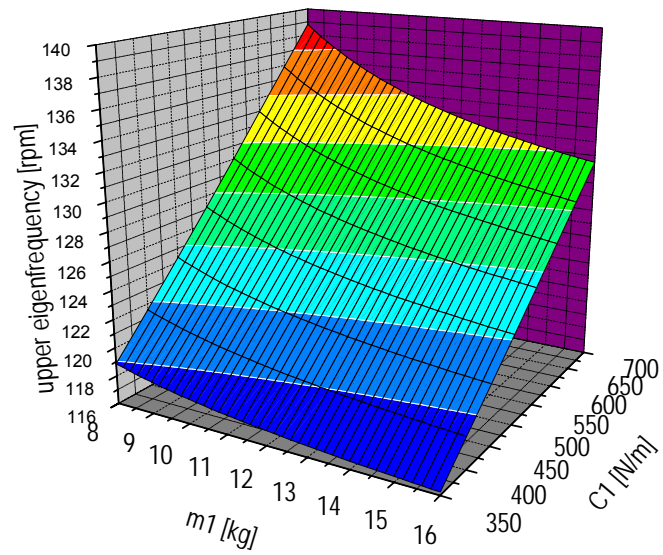
Figure 3.2-7 Influence of the Masses M_1 and M_2 as well as of the Spring Constants c_1 and c_2 on Eigenfrequency ω_1
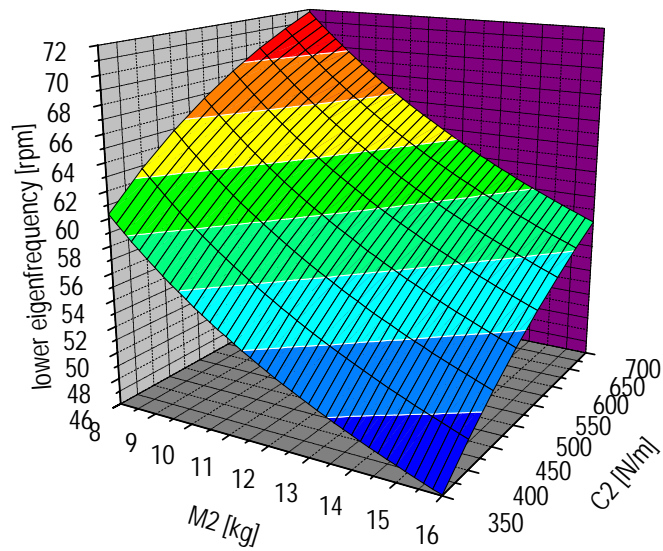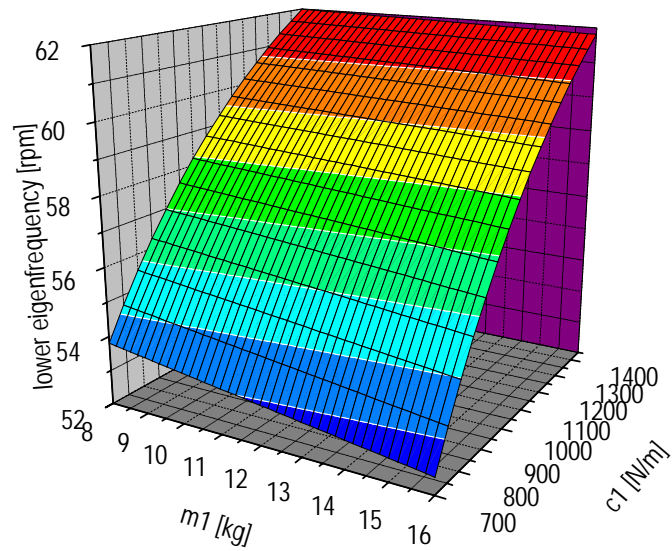
Figure 3.2-8 Influence of the Masses M_1 and M_2 as well as of the Spring Constants c_1 and c_2 on Eigenfrequency ω_1

From these figures, it can be concluded, that big masses and small spring constants are desirable. Unfortunately, for the springs along the z direction (axial direction in **Figure 3.2-5**), the springs are not only used for vibration isolation, but have also to carry the weight of the structure.

From the analysis of the available springs, it was found, that designing the sensor mounting structure to a net weight of 12 kg it is possible to reach an upper eigenfrequency in the order of 150 rpm (15 Hz). Using three springs for the support of the sensor mounting, this mass is compatible with commercial available springs with a spring constant of 0.188 N/mm and a permitted total force of 40.956 N. In order to allow the usage of the same springs, the Mass M_2 was also designed to 12 kg, using 6 springs with the same properties as described above (Construction remark: length of the loaded spring: 44.3 mm; The radial isolation is done using springs with k=0,105 N/mm with an adjusted length of 45 mm excluding the adjustment space (including adjustment space (mounting whole distance is 60 mm) 55 mm).

For the further calculation, it was assumed, that the SCR and its support structure (having a total weight of 4 kg) has an asymmetry of 1 mm (this is obviously a drastic overestimation which can only happen due to problems in the cold bearing, more realistic would be an eccentricity of 0.2 mm which could happen due to movement of the axis ant the SCR within the supporting structure). The mass of the whole experiment (including cryostat and cryostat mounting but excluding the oscillation parts) was assumed to be 50 kg.

The Matrix $\vec{\vec{\Theta}}$ can be calculated to be (note, as the formal solution is a quite complex expression, only the numeric solution is given here):

$$\vec{\vec{\Theta}} = \begin{pmatrix} 0.5773 & 0.2962 & -0.7608 \\ 0.5773 & -0.8070 & 0.1238 \\ 0.5773 & 0.5107 & 0.6369 \end{pmatrix} \tag{3.11}$$
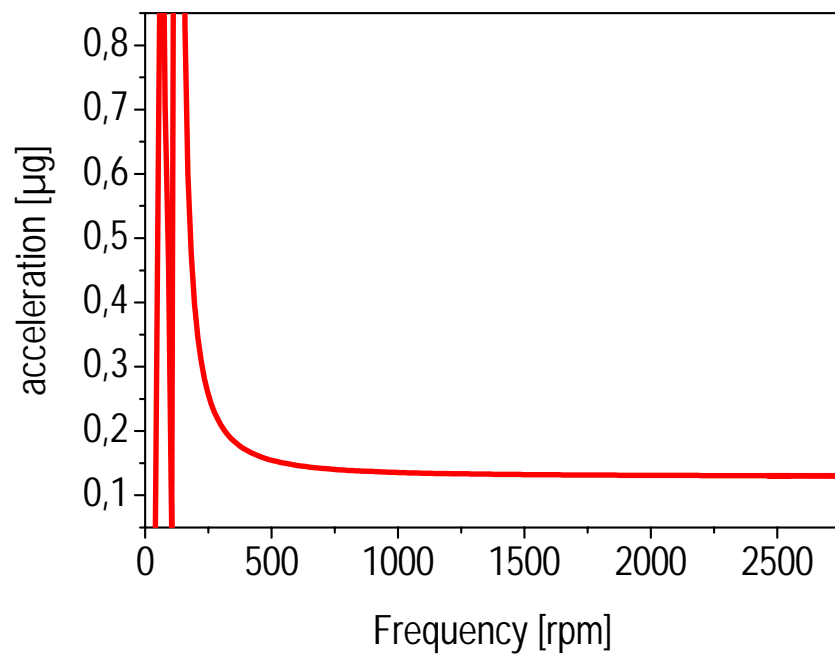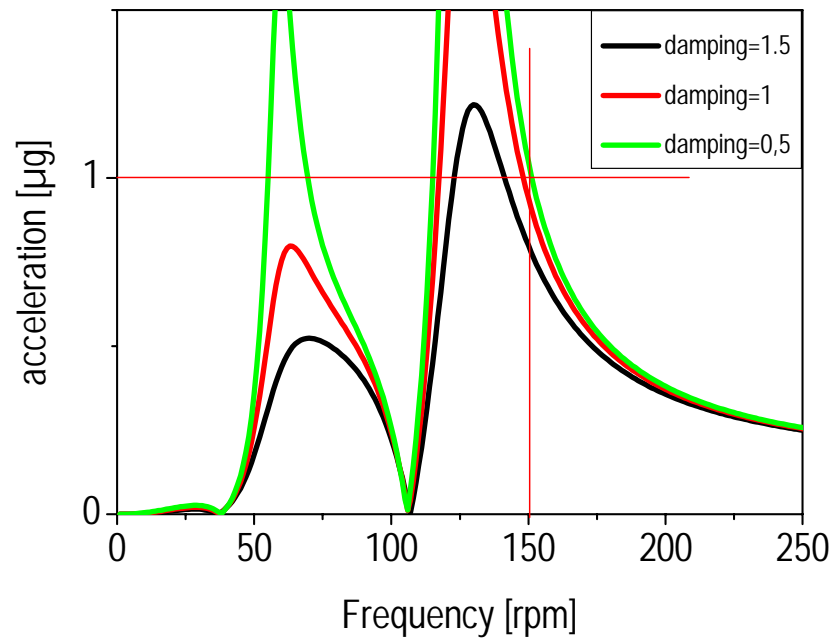
Figure 3.2-9 Low and High Frequency Part of the Acceleration Acting on the Accelerometers

It can be seen, that the noise level reaches 1 µg for motor speeds higher than 150 rpm. The graph shows the behavior for three different damping with δ_1=0.5, δ_2=1.0 and δ_3=1.5. For the high frequency part, the damping is of no importance.

The same procedure can be done for the radial components. As the springs in this case are only used for adjusting the sensor mounting, the spring constant can be chosen to be much smaller. However, it has to be noted, that the sensor-mounting acts as physical pendulum. Therefore, the position of the springs has to be chosen carefully in order to prevent excitation of rotational modes of the system. Therefore, the working point of the springs was chosen, to be below the centre of gravity of the first and the second mass. In this case, the forces acting from the radial springs act in the opposite direction from the forces caused by the axial springs, minimizing the transmitted force.

Another source of acceleration comes from the torque of the motor itself, which is a step-like function. The problem with this acceleration is that it lies in the same plane as the signal proposed to be measured. As the signal from the SCR is assumed to increase linear with the acceleration of the disc, both contributions can not be separated from each other.

The transversal stiffness of spring 1 is c_1~0.3 Nm/rad, and for c_2 the spring constant is 0.15 Nm/rad. The spring constant c_0~1Nm/rad. The moment of inertia corresponding to mass M_0=5,4 kgm². The two isolation masses have moments of inertia of approximately 0.03 kgm². The sensors are placed in a distance of 35 mm from the axis. The acceleration acting on the accelerometer due to this torque-step is shown in **Figure 3.2-10**.
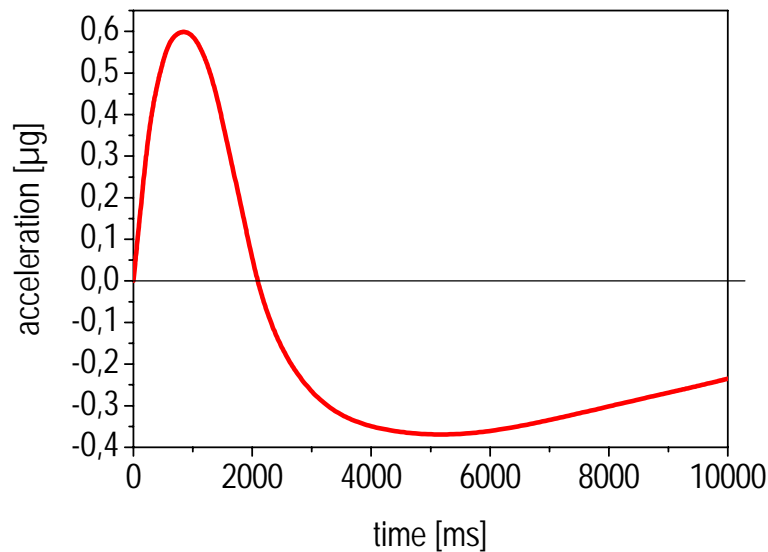
Figure 3.2-10   Acceleration acting on the accelerometer due to the step like acceleration or deceleration of the SCR. This picture was obtained by Fourier transformation of a quasi step like function, calculating the response of the system using the theory described above, and performing the inverse Fourier transformation back to time space.

It can be seen, that the acting acceleration due to the torque of the motor is less than 1 µg (even if the motor accelerates at its maximum torque). Nevertheless, this force acts irrespectively of whether the SCR is superconducting or not. Therefore calibration measurements with the SCR in the normal conducting state have to be done. Subtracting the thus obtained signals from the signals with the SCR cooled below TC eliminates the effect of this torque. Another reduction should be achieved, when subtracting the reference sensor from the signal sensor. As both sensors are placed at the same structure, the influence of the acceleration of the SCR should be strongly reduced. A careful analysis of this topic has to be done during the experiment.

Note, that this calculation is based on the assumption, that the whole structure is only 50 kg in weight, and is moving free in the air. When attaching a heavy ground plate, and fixing this plate with isolation elements to the laboratory ground, the influence can also be strongly decreased.

The spring adjustment is shown in **Figure 3.2-11**
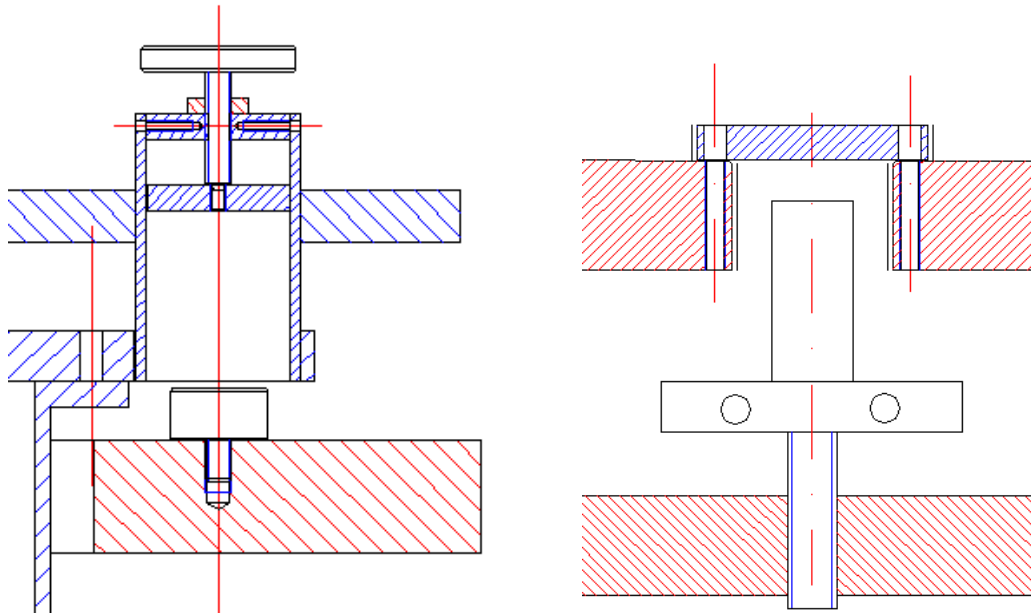
Figure 3.2-11 Spring adjustment. The two designs are the two axial adjustments, the radial adjustment is similar to the left figure.

3.3 Thermal Design

The calculation of the thermal properties is based on the formulas given in the VDI Wärmeatlas[28].
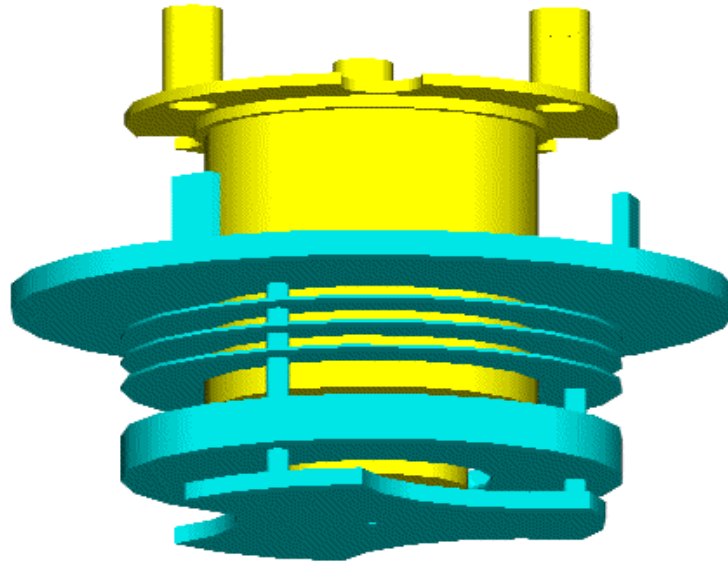

Figure 3.3-1   Sketch of the thermal relevant parts of the experimental setup.

The thermal isolation of the system has to fulfill two demands: first, the SCR has to be cooled well below T_C, and second, the accelerometers have to be placed in a (nearly) room temperature ambient (the temperature will be measured using PT 100 resistors for the three principal positions, each sensor will be placed in the vicinity of one to two PT 100 used for heating of the sensor surrounding keeping the sensor at room temperature). Therefore it was decided to place the accelerometers in a vacuum chamber equipped with a multilayer insulation. In the remaining space between cryostat and accelerometer cage, three to four radiation shields have to be placed. The cooling is done by pumping the cryogenic gas along the experimental setup. In order to constrict the costs of the coolant, a maximal cooling power of about 30 W@4.2 K should not be exceeded.

From the principal properties of a <u>multilayer insulation</u> (MLI), it can be assumed, that a maximum heating power of 12 W/m² for a temperature gradient of approximately 300 K (LHe cooling) can be reached. The whole surface of the sensor structure is about 0.1m², resulting in a thermal load of

about 1.2 W. This heat has to be cooled away on one side, but also to be supplied at the sensor mounting. This will be done using PT100 resistors.

In order to have some safety margin, for the further considerations, a thermal power of **3 W through the MLI** will be assumed.

The <u>thermal radiation</u> using four radiation shields is calculated by

$$\dot{q}_R = \sigma(T_h^4 - T_l^4) \frac{1}{\frac{2}{\varepsilon} - 1} \frac{1}{N+1} A \tag{3.12}$$

with T_h and T_l being the highest and lowest temperature. For this case, T_h=300 K and T_l=4.2 K is assumed. The Stefan Bolzmann constant σ=5.67W/(m²K⁴). The reflectivity of the radiation shields is assumed to be ε=0.2. Using 4 shields with an area of A=0.05 m², the **thermal power due to radiation is approximately 1 W** (Note that the reflectivity of 0.2 is an underestimation, applying ε=0.1 reduces the radiation power to 0,5 W).

The <u>heat conductance in the N_2 (He) gas</u> is calculated using

$$\dot{q}_G = \lambda \frac{l}{A} \Delta T \tag{3.13}$$

with a thermal conductivity of the gas of approximately 0,084 Wm/K. The conducting area is the same as introduced in the calculation of the radiation. The length of the isolation shield is 100 mm (0.1 m). therefore, the thermal power from the **thermal conductivity of the gas is approximately 13 W.**

The heat conductance in the remaining structural parts is calculated using the same equation as given for the thermal conductance in the gas (However with changed cross-sections. The total cross section (including the axis, and the structural material needed for the support of the SCR and the radiation shields is A=0.003m². Therefore, the **heat transport through the structural material is approximately 4 W**.

The total heat transport through the experiment (neglecting the cryostat itself) is about 21 W, which is in the order of the design goal of the experiment. As the specific heat of N_2 is approximately 1 kJ/kg.K (for He its ~5.2 kJ/kg.K), the density of the gas is approximately 2 kg/m³ for N_2 (2 kg/m³ for He).

Both liquids have a density of approximately 1000 Kg/m³ at low temperature. Therefore, the gas/liquid fraction is approximately 260 for He, and 400 for LN_2. in order to reach a cooling of 30 W and a temperature of ~7 K (LHe, ; ΔT=5 K, lowering of boiling temperature neglected) and ~80 K (LN_2; ΔT=10 K, lowering of boiling temperature ~12 K), a consumption of 0,9 m³/h He-gas and a consumption of 3.8 m³/h N_2 gas is necessary, resulting in a consumption of 3.,5 liter LHe/h and 4.5 liter LN_2/h. Therefore, the cryostat has to be capable to cover at least 30 l for a proper cooling and operation of the experiment.

3.4   Magnetic Fields

In order to subject the superconducting ring to an external magnetic field, a coil will be inserted in the experiment (see **Figure 3.4-1**). The coil can be removed completely without serious changes.
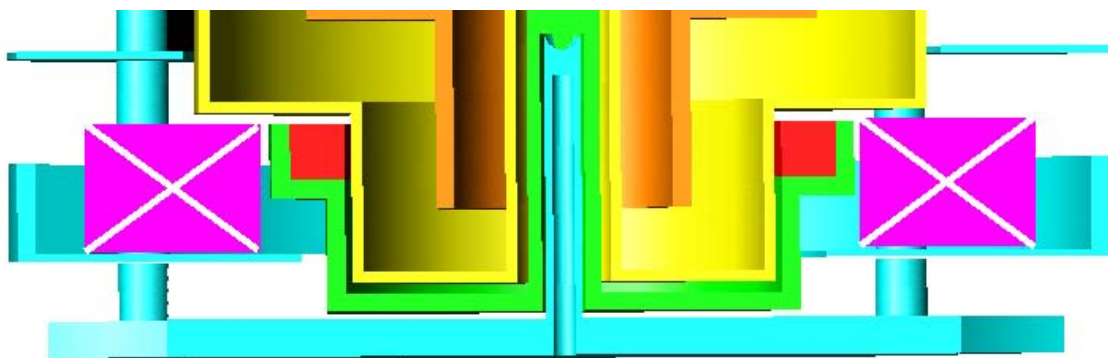
Figure 3.4-1   Magnetic field coil inside the experiment

Coil Parameters	Requirement
Strand diameter	1.5 mm
Number of winding	660
Cross section of coil	1665 mm²
Resistance at 77 K	0.5 Ω
Resistance at RT	4.8 Ω
Maximum current	8A
Maximum field	65 mT

Table 3   Performance of the coil
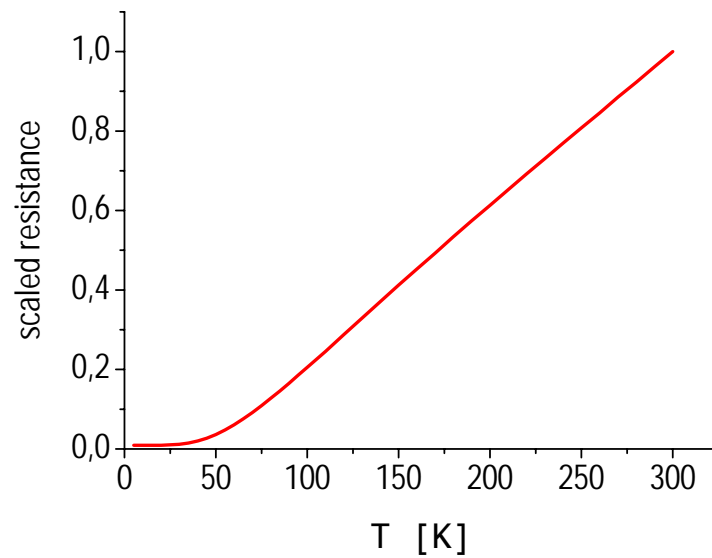
Figure 3.4-2   Resistance of copper as a function of temperature. The Debye temperature of copper is assumed to be 343 K. The room temperature conductivity is 100 %IACS corresponding to 58 MS/m.
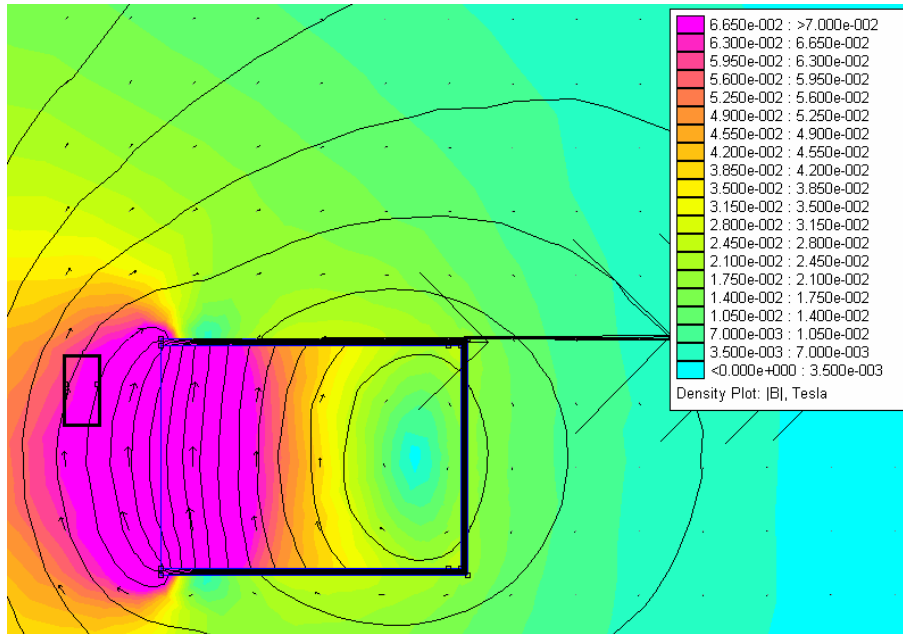
Figure 3.4-3 Calculation of the magnetic field distribution

The parameters of the coil are given **Table 3**. The change in the resistance due to the lowered temperature can be estimated from **Figure 3.4-2** . The maximum magnetic field (for operation at 8 A) was calculated to be 65 mT (see**Figure 3.4-3**). In order to reach this field, the coil has to be shielded by silicon core iron (without shielding the field is reduced to 45 mT).

Operating the coil at the given parameters results in an heat production of ~33 W yielding an additional coolant consumption of ~6l/h. The situation becomes better when cooling to lower temperature (e.g. Helium temperature), where the resistance is lowered to about 0.05 Ω resulting in an additional coolant consumption of 1 l/h.

The magnetic signal of the superconductor resulting from the London moment will be measured using a DC Milligauss Magnetometer produced by AlphaLab Inc. The Gauss-meter has a resolution of 1 nT, and a full range of 200 µT. For the measurement of the magnetic field produced by the field coil, commercially available hall-probes will be used.

3.5   Electric connectors

In order to read the signal of the accelerometers, a 20 pin electric connection is needed. For the temperature control of the accelerometers, additional 8 pins are needed. For the Gauss-meter and the Hall probe additional 12 pins are needed. Therefore, two LEMO-vacuum connectors with 22 pins each will be used (HGP.4S.322.CLLPV). Using these connectors, a spare of 4 pins to the vacuum chamber is available for later upgrades, or improvements of the electric design.

3.6 Expected Performance in Laboratory Environment

The expected performance based on the design outlined in the chapters before is summarized in **Table 4**, which is fully compliant to the requirements.

	Requirement	Expected Performance
Resolution of Acceleration Sensor	1 µg	0.3 µg
Angular Acceleration of Superconductive Ring	> 200 s^{-2}	380 s^{-2} Peak: 1700 s^{-2}
Minimum Measurement Time	1 s	3 s
Maximum Rotational Speed of Superconductive Ring	3000 rpm	> 3000 rpm 5800 rpm are possible (the mechanical stability has to be checked)
Temperature of Superconductive Ring	< 77 K	70 K

Table 4 Summary of Requirements and Expected Performance for Experimental Facility

4 TEST PLANS

4.1 Test Plan for Validation of Design

As the goal which should be reached by this experiment are quite challenging, an extensive test phase for the validation of the experiment has to be performed before running the actual experiments.

1) During the manufacturing of the experimental parts, the accelerometers should be placed where the experiment should be carried out. A long term monitoring of the vibrations of the surrounding, as well as a test of the stability of the accelerometers should be gained from this. As three accelerometers are measuring the same direction, the differences between the accelerometers can be checked (the axes of the accelerometers should be changed in that way, that there is a period for which each accelerometer has measured the same direction as an any other). Special care should be taken to the periods which are of particular interest for the experimental phases (late night and weekend).

2) The mechanical stability of the rotational system has to be checked. Therefore a dummy ring with the same mass has to be placed in the position of the SCR. The accelerometers must not be mounted at this time. Several acceleration and acceleration tests should be done. The first test shall be done at room temperature, to permit full access to the structure. Later tests shall be done at cryogenic temperature to identify possible thermal problems before the experiment. The heat control system A and D has to be installed.

3) In the meantime, the evacuated sensor mounting can be tested if the isolation is sufficient to prevent the accelerometers from thermal destruction (therefore the heat control system B and C have to be installed).

4) Finally, a test with the dummy superconductor should be done, to check the influence of the vibrations and the acceleration of the superconductor on the accelerometers (see **Figure 3.2-9** and **Figure 3.2-10**). This test could also be done using the already mounted superconductor. The decision if the dummy or the real conductor will be used will be taken after tests 1 - 3. One of the results of this test should also be the time between two accelerations which is necessary to allow the decay of oscillations.

4.2   Test Plan for Experiment

For the experimental case, it is proposed to start at the lowest temperature achievable with the experiment at liquid nitrogen. The signal of the superconducting ring when decelerating from a mean rotational speed (which has to be taken from the validation tests) should be measured, starting with a low deceleration speed (due to safety considerations). The same test should be performed with the same acceleration (the same value of angular acceleration but opposite sign). Subsequently, the experiment should be repeated with increasing acceleration (deceleration) speed up to the upper safe limit of the experiment obtained from the validation phase.

The same procedure should be repeated at several temperatures till the normal conducting state of the superconductor is reached. As the design of the experiment should also allow to perform experiments at lower temperatures, it is proposed to perform also some experiments using the HTC ring at temperatures below 50 K (see **Figure 2.2-5**). This experiments would require liquid He, as nitrogen solidifies at 63 K, therefore a temperature lowering using the enthalpy of evaporation stops at temperatures higher than around 70 K (or at least the cooling power converges toward zero).

5 REFERENCES

[Airmotors]   http://www.duesterloh.de/deutsch/hydraulikmotoren/hydraulikmotoren.html

http://www.dynatork.co.uk/index_flash.htm

http://www.kinequip.com/airmotors.asp?Cat_Id=9#

http://www.psiautomation.com/

Private communication

[Applied Mems] http://www.appliedmems.cc/htmlmems/p_si_flex.html; private communication

[Böge 1989] Böge A, Das Techniker Handbuch – Band 1; Vieweg&Sohn (1989)

[De Matos et al. 2001] De Matos, C. J., and Tajmar, M., "Gravitomagnetic Barnett Effect", *Indian Journal of Physics* **75B**(5), 2001, pp. 459-461 (also gr-qc/0012091)

[Escher et al. 1996] Escher U., Samuel R., Gladun A., Hegenbarth E., The influence of $SrSo_4$ additives to $Bi_2Sr_2CaCu_2O_8$ high temperature Superconductors. Physica B **219-220** (1996), 189-191

[Hense 1999/2002] Hense K, Gitterdynamik in der orthorhombischen Struktur YCu_2, TU Wien Diplomathesis 1999

Hense K, CEF phonon interaction in the orthorhombic compound $NdCu_2$, TU Wien, PhD thesis 2002

[Hense 2002] Hense K et al. Influence of the annealing time of internal tin Nb_3Sn strands on the critical current and the magnetization losses; Physica C **372-276** (2002) pp 1758-1761

[Hense 2004] Hense K. et al., Scaling behavior for the exponents of U–I-, U–B- and U–T – measurements, Physica C **401** (2004) 214-217

[Honeywell] http://www.inertialsensor.com/qa3000.shtml ; private communication

[Keithley] http://www.keithley.com/main.jsp?action=keithleysearch

[MWS] http://www.mws-sensorik.de/pdf/5401.pdf ; private communication

[Silicon Designs] http://www.silicondesigns.com/1221.html; private communication

[Tajmar et al. 2001] Tajmar, M., de Matos, C.J., "Coupling of Electromagnetism and Gravitation in the Weak Field Approximation", *Journal of Theoretics*, **3**(1), February 2001 (also gr-qc/0003011)

[Tajmar et al. 2003] Tajmar, M, de Matos, C. J., "Gravitomagnetic field of a rotating superconductor and of a rotating superfluid", *Physica C*, **385**, 2003, pp. 551-554

[Tate et al. 1989] Tate, J., Cabrera, B., Felch, S.B., Anderson, J.T., "Precise Determination of the Cooper-Pair Mass", *Physical Review Letters*, **62**(8), 1989, pp 845-848

[Tate et al. 1990] Tate, J., Cabrera, B., Felch, S.B., Anderson, J.T., "Determination of the Cooper-Pair Mass in Niobium", *Physical Review B*, **42**(13), 1990, pp 7885-7893

[Torquesystems] http://www.torquesystems.com; private communications

[VDI1997] VDI Wärmeatlas; Springer Verlag Berlin Heidelberg (1997)

DISTRIBUTION LIST

AFRL-MN-EG-TR-2007-7012

Defense Technical Info. Center   1
8725 John J. Kingman Rd Ste 0944
Fort Belvoir VA 22060-6218

Eglin AFB offices:

AFRL/MNOC-1 (STINFO Office)   1
AFRL/MN CA-N   1
AFRL/MNME   1
AFRL/MNMF   1
AFRL/MNMW   1
AFRL/MNMI   1